A&A 485, 377–393 (2008)
DOI: 10.1051/0004-6361:20078993

Astronomy & Astrophysics

Lines in the cosmic microwave background spectrum from the epoch of cosmological helium recombination

J. A. Rubiño-Martín[1], J. Chluba[2], and R. A. Sunyaev[2,3]

[1] Instituto de Astrofisica de Canarias (IAC), C/Via Lactea, s/n, 38200, La Laguna, Tenerife, Spain
e-mail: jalberto@iac.es
[2] Max-Planck-Institut für Astrophysik, Karl-Schwarzschild-Str. 1, 85741 Garching bei München, Germany
e-mail: jchluba@mpa-garching.mpg.de
[3] Space Research Institute, Russian Academy of Sciences, Profsoyuznaya 84/32, 117997 Moscow, Russia

Received 5 November 2007 / Accepted 29 February 2008

ABSTRACT

The main goal of this work is to calculate the contributions of bound-bound transitions of helium to the cosmological recombination spectrum. We show that helium in the early Universe causes unique features to appear in the total cosmological recombination spectrum. These may provide a unique observational possibility to determine the relative abundance of primordial helium, well before the formation of first stars. We include the effect of the tiny fraction of neutral hydrogen atoms on the dynamics of He II → He I recombination at redshifts $z \sim 2500$. As discussed recently, this process significantly accelerates He II → He I recombination, resulting in rather narrow and distinct features in the associated recombination spectrum. In addition this process induces some emission within the hydrogen Lyman-α line, before the actual epoch of hydrogen recombination around $z \sim 1100$–1500. We also show that some of the fine-structure transitions of neutral helium appear in absorption, again leaving unique traces in the cosmic microwave background blackbody spectrum, which may allow confirmation of our understanding of the early Universe and of detailed atomic physics.

Key words. atomic processes – cosmology: cosmic microwave background – cosmology: theory – cosmology: early Universe

1. Introduction

The recombination of helium hardly influences the cosmic microwave background (CMB) angular fluctuations, as measured with success by WMAP (Bennett et al. 2003), since it occurred well before the Thomson visibility function defined by hydrogen recombination (Sunyaev & Zeldovich 1970) reaches its maximum. However, similar to the release of photons during the epoch of cosmological hydrogen recombination (Rubiño-Martín et al. 2006; Chluba et al. 2007; Chluba & Sunyaev 2006a), one does expect some emission of photons by helium, and the main goal of this paper is to calculate the contributions of bound-bound transitions of helium to the cosmological recombination spectrum.

In our recent papers we computed the detailed cosmological recombination spectrum of hydrogen resulting from bound-bound (Rubiño-Martín et al. 2006; Chluba et al. 2007) and bound-free (Chluba & Sunyaev 2006a) transitions between atomic levels, including up to 100 shells, also taking into account the evolution of individual energetically degenerate angular-momentum substates. We followed the ideas and suggestions of earlier investigations (Zeldovich et al. 1968; Peebles 1968; Dubrovich 1975; Bernshtein et al. 1977; Beigman & Sunyaev 1978; Rybicki & dell'Antonio 1993; Dubrovich & Stolyarov 1995; Burgin 2003; Dubrovich & Shakhvorostova 2004; Kholupenko et al. 2005; Wong et al. 2006). Observations of these recombinational lines might provide an additional unbiased way of *directly* determining the baryon density of the Universe (e.g. see Dubrovich 1975; Bernshtein et al. 1977; or more recently Kholupenko et al. 2005; Chluba & Sunyaev 2007b) and of obtaining some additional information about the other key cosmological parameters, facing different degeneracies and observational challenges.

Obviously, direct evidence of the emission of extra ~5 photons per recombining hydrogen atom (Chluba & Sunyaev 2006a) will be *unique proof* of the completeness of our understanding of the processes occurring at redshifts $z \sim 1400$, i.e. before the CMB angular fluctuations were actually formed. From this point of view, an observation of lines emitted during He III → He II close to $z \sim 6000$ and He II → He I around $z \sim 2500$ will be an even more impressive confirmation of the predictions within the standard hot big bang model of the Universe, realizing that nowadays exact computations using the full strength of atomic physics, kinetics, and radiative transfer in principle should allow prediction of the cosmological recombination spectrum from both epochs with very high precision.

The first attempt to estimate the emission arising from helium recombination was made by Dubrovich & Stolyarov (1997). However, only now are detailed numerical computations becoming feasible and only now have atomic physicists begun to publish *accurate* and *user-friendly* transition rates (Drake & Morton 2007; Beigman & Vainshtein 2007) for neutral helium, including singlet-triplet transitions, which very strongly influence the recombination of helium.

According to computations of nuclear reactions in the early Universe (Olive & Steigman 1995; Cyburt 2004), the abundance of helium is close to 8% of the number of hydrogen atoms, so naïvely only small additional distortions of the CMB blackbody spectrum due to helium recombination are expected. However, for helium there are *two* epochs of recombination, resulting in

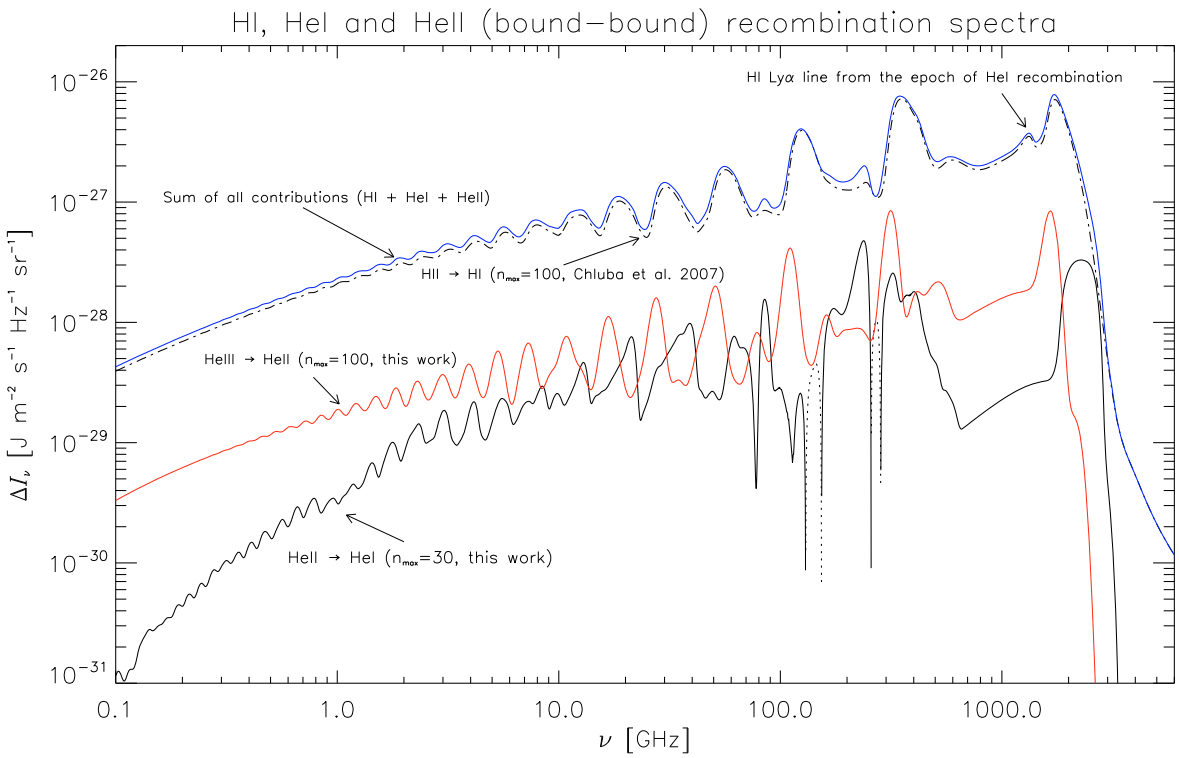

Fig. 1. Full helium and hydrogen (bound-bound) recombination spectra. The following cases are shown: (a) the He II → He I recombination spectrum (black solid line), which has been obtained by including up to $n_{\rm max} = 30$ shells, and considering all the J-resolved transitions up to $n = 10$. In this case, there are two negative features, which are shown (in absolute value) as dotted lines; (b) the He III → He II recombination spectrum (red solid line), where we include $n_{\rm max} = 100$ shells, resolving all the angular momentum sublevels and including the effect of Doppler broadening due to the scattering off free electrons; (c) the H I recombination spectrum, where we plot the result from Chluba et al. (2007) up to $n_{\rm max} = 100$. The H I Lyman-α line arising in the epoch of He I recombination is also added to the hydrogen spectrum (see the feature around $\nu = 1300$ GHz). In all three cases, the two-photon decay continuum of the $n = 2$ shell was also incorporated. Feedback processes for He II and He I recombinations are not taken into account. The blue line shows the total recombination spectrum.

at least a doubling of the possible number of additional photons. Furthermore, He III → He II recombination is very fast, particularly since there is a large quasi-constant amount of free electrons belonging to hydrogen (Dubrovich & Stolyarov 1997). This implies that photons are emitted in a much shorter period, so that more narrow features are produced[1]. It is also very impressive that the He III → He II recombination lines practically coincide and therefore amplify the corresponding hydrogen line (see Fig. 1). This is because the difference in the redshifts of the two recombinations is close (∼4.3), whereas the energy of similar transitions scales as $Z^2 = 4$ for He II, such that the two effects practically compensate each other.

The spectral distortion due to He II → He I recombination should have a completely different character. First, for small n neutral helium has a much more complicated spectrum than hydrogenic atoms (e.g. highly probable fine-structure transitions). In addition, the ratio of the energies for the second and first shell is ∼2.1 times higher than for hydrogenic atoms, while the energies of the highly excited levels are very close to hydrogenic. Since the transitions from the second to the first shell control helium recombination, this leads to the situation in which even for transitions between highly excited levels the corresponding $\Delta n = 1$-lines do not coincide with those emitted during hydrogen or He III → He II recombination.

It will also be shown below (Sect. 5) that in the recombination spectrum some fine-structure lines become very bright, and that two of them actually appear in *absorption*. These features lead to additional non-uniformities in the spectral variability structure of the *total* CMB spectral distortion from recombination, where some maxima are amplified and others are diminished. This may give rise to a unique possibility of separating the contributions from helium and hydrogen, thereby *allowing us to measure the pre-stellar abundance of helium in the Universe*. Until now not even one *direct* method for such a measurement is known.

For the computation of the recombination helium spectrum we are crucially dependent on the recombination history of helium and additional processes that strongly affect the standard picture. In this context, probably the most important physical mechanism is connected with the continuum absorption of the permitted 584 Å and intercombination 591 Å line by a very small amount of neutral hydrogen present in ionizational equilibrium during the time of He II → He I recombination (Hu et al. 1995; Switzer & Hirata 2007a; Kholupenko et al. 2007). Switzer & Hirata (2007a) and Kholupenko et al. (2007) have recently carried out the first detailed analysis of this problem and have included it for the computations of the He II → He I recombination history, showing that the recombination of neutral helium is significantly faster. Here we reanalyse this process, and discuss in detail certain physical aspects of the escape problem in the aforementioned lines.

We first consider two "extreme" cases for the escape problem that can be treated analytically: (i) where line scattering leads to *complete redistribution* of photons over the line profile; and

[1] As we will demonstrate here, even the scattering of photons by free electrons cannot change this conclusion (see Sect. 5.5).

(ii) where there is *no redistribution*[2]. Moreover, we develop a useful 1D integral approximation for the escape probability that permits us to treat any of these two cases without increasing the computation time significantly. Our final results for the escape probability in the more realistic case of *partial redistribution* (or equivalently for coherent scattering in the restframe of the atom) are based on detailed numerical computations that will be presented in a separate paper (Chluba et al. 2008, in preparation). One can then obtain a sufficiently accurate description of the real dynamics by *fudging* the escape probability using the "no redistribution" case mentioned above with a certain function that can be obtained by comparison with full numerical computations. Our final results for the escape probability are in very good agreement with those obtained by Switzer & Hirata (2007a) (see discussion in Sect. 3).

Interestingly, the hydrogen continuum process leaves additional distinct traces in the cosmological recombination spectrum because the continuum absorption of the He I photons leads to significant early emission in the H I Ly-α transition at $\nu \sim 1300\,\mathrm{GHz}$, well separated from the Ly-α line originating during hydrogen recombination at $\nu \gtrsim 1500\,\mathrm{GHz}$, and containing about 7% of all photons that were released in the hydrogen $2p$–$1s$ transition. The amplitude and width of this feature is completely determined by the conditions under which the above process occurs.

The main results of this paper are the bound-bound spectra of He II and He I from the epoch of cosmological recombination (see Fig. 1). The strongest additions to the cosmological hydrogen recombination spectrum due to the presence of helium lines reach values up to 30–40% in several frequency bands. This strongly exceeds (roughly by a factor of four) the relative abundance ratio of helium to hydrogen, raising hopes that these distortions will be found once the recombination lines become observable.

It is important to note that for the computations in this paper (see Fig. 1) we do not include the impact of feedback processes on the computed recombination lines. Among all the possible feedback mechanisms, the most relevant for the recombination spectrum is the pure continuum absorption (far from the resonances) of the remaining He I $2^3\mathrm{P}_1 - 1^1\mathrm{S}_0$ intercombination-line and He I $2^1\mathrm{P}_1 - 1^1\mathrm{S}_0$ photons. Because of this process, these photons will be finally absorbed, and the corresponding features on the final spectrum will disappear, producing additional photons that will emerge mainly through the Lyα line in the hydrogen spectrum.

2. Basic equations. The helium atom

A description of the basic formalism and equations for calculating the time evolution of the populations for different atomic species (hydrogen or helium) within a multi-level code during the epoch of cosmological recombination ($800 \lesssim z \lesssim 7000$) can be found in Seager et al. (2000). In this paper, we follow the same approach and notation as used in our previous works for the computation of the hydrogen recombination spectrum (Rubiño-Martín et al. 2006; Chluba et al. 2007). The codes used for the computations presented here were obtained as an extension of the existing ones by including the equations for the population of the He I and He II levels. As in our previous works, we developed two independent implementations in order to double-check all our results.

For all the results presented in this paper we use the same values of the cosmological parameters adopted in our previous works, namely (Bennett et al. 2003): $\Omega_\mathrm{b} = 0.0444$, $\Omega_\mathrm{tot} = 1$, $\Omega_\mathrm{m} = 0.2678$, $\Omega_\Lambda = 0.7322$, $Y_\mathrm{p} = 0.24$ and $h = 0.71$.

2.1. He I model atom

In our computations we follow in detail the evolution of the level populations in neutral helium, including up to $n_\mathrm{max} = 30$ shells. For all levels, we distinguish between "singlet" ($S = 0$) and "triplet" ($S = 1$) states. Up to $n = 10$, we follow separately all levels with different total angular momentum J. This permits us to investigate in detail the fine structure lines arising from cosmological recombination. Above $n = 10$, we do not resolve J quantum number, and only LS-coupling is considered. Each level is quoted using the standard "term symbols" as $n^{2S+1}L_J$, and spectroscopic notation is used. When considering J-resolved levels, the degeneracy factor is given by $g_i = (2J + 1)$, while in opposite case we would have $g_i = (2S + 1)(2L + 1)$.

To define our model atom completely, we need to specify for each level $i = \{n, L, S, J\}$, the energy, E_i, and photoionization cross-section, $\sigma_{ic}(\nu)$, as a function of frequency, which is important in order to account for the effect of stimulated recombination to high levels. Finally, a table with the Einstein coefficients, $A_{i\rightarrow j}$, and the corresponding wavelengths for all the allowed transitions has to be given.

2.1.1. Energies

The energies for the different levels up to $n = 10$ are taken from Drake & Morton (2007). However, this table is not absolutely complete, and some of the high L substates for outer shells are missing. In order to fill this table up to $n_\mathrm{max} = 30$, we proceed as follows. We use the formulae for quantum defects (see Drake 1996, Chap. 11) to compute the energies of all terms with $L \leq 6$ and $n > 10$. For all other levels, we adopt hydrogenic values for the energies, using $-R_\mathrm{H}/n^2$, with $R_\mathrm{H} \approx 13.6\,\mathrm{eV}$. Note that, in this last case, the energy levels will be degenerate in L and J. However, this approximation is known to produce very good results (Beigman & Vainshtein 2007). A summary of the final energies adopted for each particular level in our He I model atom is shown in Fig. 2, both for the singlet and triplet states.

2.1.2. Photoionization cross-sections

For $n < 10$, the photoionization cross-sections, $\sigma_{ic}(\nu)$, are taken from the TOPbase[3] database (Cunto et al. 1993). We note that this database does not contain J-resolved information and only cross-sections for $L \leq 3$ can be found. To obtain J-resolved cross-section we assume that the cross-section for each sublevel is identical, i.e.

$$\sigma_{\{n,L,S,J\}\rightarrow c}(\nu) = \sigma_{\{n,L,S\}\rightarrow c}(\nu).$$

There are two important issues that we would like to stress. First of all, there are large gaps in the tables from TOPbase. We computed the missing cross-sections up to $n = 5$ using the expressions from Smits (1996) and Benjamin et al. (1999) for spontaneous photo-recombination rates to infer the photoionization rates R_{ic}. With this procedure it is not possible to include the effect of stimulated recombination self-consistently.

[2] In this case, line scattering is totally coherent in the lab frame. During recombination this is a very good approximation for the very distant wings of the line.

[3] At http://vizier.u-strasbg.fr/topbase/topbase.html

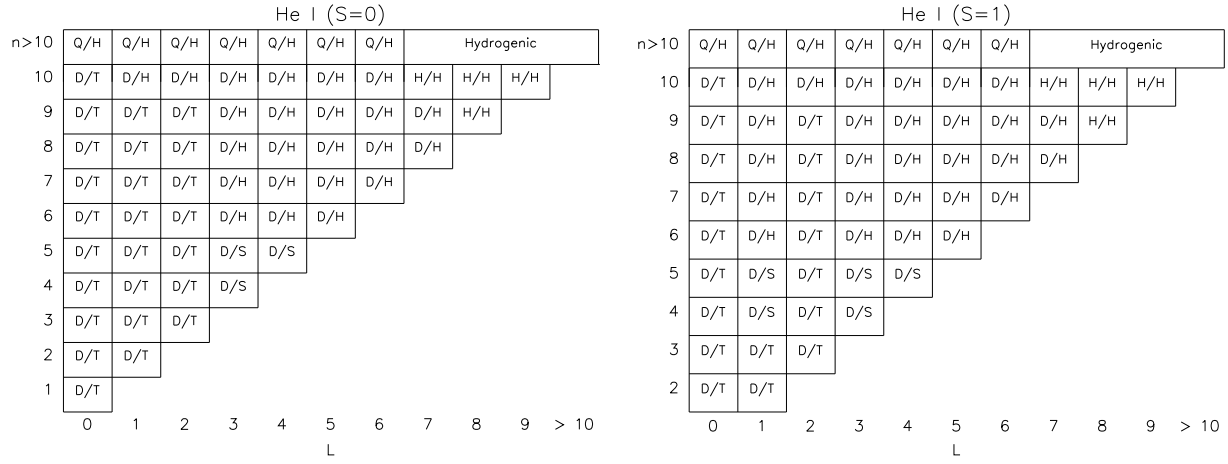

Fig. 2. Graphical representation of the values adopted for the energies and photoionization cross-sections of our He I model. For each level, two letters are given that refer to the energy and the photoionization cross-section of that level, respectively. For the energies, the letters refer to: "D": Drake & Morton (2007); "Q": quantum defect expansions Drake (1996); and "H": hydrogenic approximation. For the photoionization cross-sections, the letters refer to: "T": TOPbase; "S": Smits (1996); Benjamin et al. (1999); and "H": re-scaled hydrogenic values.

We estimated the errors due to this effect using the replacement $R_{ic} \rightarrow R_{ic} \times [1 + n_{bb}(\nu_c)]$, where $n_{bb}(\nu_c)$ is the blackbody photon occupation number at the ionization threshold of the level, and found changes of 10−20%. For all other levels we follow Bauman et al. (2005) and adopt re-scaled hydrogenic cross-section. This is done using our computations of $\sigma_{ic}(\nu)$ for the hydrogen atom (based on Karzas & Latter 1961; Storey & Hummer 1991) and shifting the threshold frequency accordingly.

Secondly, we would like to point out that the cross-sections provided in TOPbase are sparsely sampled. For example, the power-law behaviour up to twice the threshold frequency is usually given by ∼10 points. Furthermore, due to auto-ionization several resonances exist at large distances above the ionization threshold, and many of these extremely narrow features are represented by one point. Fortunately, because of the exponential cut-off from the blackbody spectrum these resonances do not significantly affect R_{ic}. Still, we estimate the error budget using these cross-sections to be ∼10%.

A summary of the final values adopted for each particular level in our He I model atom is also shown in Fig. 2. We finally note that, in order to speed up our computations, we tabulate the photoionization rate during the initialization state of our codes, which involves one-dimensional integral over the (blackbody) ambient photon field, and we interpolate over this function when needed. At every particular redshift, the corresponding photorecombination rate is computed using the detailed balance relation, which is satisfied with high precision due to the fact that at the redshifts of interest, the electron temperature and the radiation temperature practically do no differ.

2.1.3. Transition probabilities

Our basic database for the transition probabilities is taken from Drake & Morton (2007), which is practically complete for the first ten shells and includes 937 transitions between J-resolved states. This database also contains spin-forbidden transitions (i.e. singlet-triplet and triplet-singlet), which take into account the mixing of singlet and triplet wave functions.

However, there are some transitions missing in these tables that involve lower levels with $n \geq 8$ and $L \geq 7$ for the singlet, and $n > 7$ and $L > 6$ for the triplet states. These gaps are filled using rescaled hydrogenic values as follows: for a given transition $\{n, L, S, J\} \rightarrow \{n', L', S', J'\}$, we first obtain the non-J-resolved transition probability $A^{\rm He}_{nL \rightarrow n'L'}$ scaling by the ratio of the transition frequencies to the third power. Whenever J-resolved information for the level energies is available, we also compute the weighted mean transition frequency. However, the corresponding corrections are small. To obtain the final estimate for the J-resolved value, we assume that

$$A^{\rm He}_{nLJ \rightarrow n'L'J'} = \frac{(2J'+1)}{(2L'+1)(2S'+1)} A^{\rm He}_{nL \rightarrow n'L'}. \quad (1)$$

These expressions are also used to include all transitions involving levels with $n, n' > 10$ and for those between the $n > 10$ and $n' \leq 10$ states, the corresponding average over J and J' being adopted. For the case of $n_{\rm max} = 30$, our final model contains 80 297 bound-bound transitions.

Finally, we note that once the energies of all levels are obtained, the wavelengths for all transitions are calculated consistently using the respective upper ($E_{\rm u}$) and lower ($E_{\rm l}$) energy levels as $\nu_{\rm ul} = (E_{\rm u} - E_{\rm l})/h$. This is important in order to guarantee that we recover the correct local thermodynamic equilibrium solution at high redshifts (see discussion in Sect. 3.2.1 of Rubiño-Martín et al. 2006).

2.1.4. Two-photon decay and non-dipole transitions

Apart from the aforementioned transitions, we also include in our computations the two-photon decays of the $2^1{\rm S}_0$ and $2^3{\rm S}_1$ levels. We adopt the values $A_{2^1{\rm S}_0 - 1^1{\rm S}_0} = 51.3\ {\rm s}^{-1}$ and $A_{2^3{\rm S}_1 - 1^1{\rm S}_0} = 4.09 \times 10^{-9}\ {\rm s}^{-1}$ (Drake et al. 1969).

Our final spectrum also contains the contribution of the $2^1{\rm S}_0$ two-photon decay spectrum, which is computed as for the hydrogen case (see, for example, Eq. (3) in Rubiño-Martín et al. 2006). The fit to the profile function (Drake 1986) for this transition is taken from Switzer & Hirata (2007a).

We also included some additional low probability non-dipole transitions (Łach & Pachucki 2001), but in agreement with previous studies we found them to be negligible.

2.2. The He II model atom

For singly ionized helium we use hydrogenic formulae (see, for example, Rubiño-Martín et al. 2006) with re-scaled transition

frequencies (see also Switzer & Hirata 2007a). The 2 s two-photon decay profile is modelled using the one for hydrogen, adopting the (re-scaled) value of $A^{\rm HeII}_{2s\to1s} = 526.5\ {\rm s}^{-1}$.

3. Inclusion of the hydrogen continuum opacity

In order to include the effect of absorption of photons close to the optically thick resonant transitions of helium during He II → He I recombination due to the presence of neutral hydrogen, one has to study in detail how the photons escape in the helium lines. This problem has been solved by two of us using a diffusion code, and the results will be presented in a separate paper (Chluba & Sunyaev 2008, in preparation).

For the purposes of this paper, the important conclusion is that the results obtained using this diffusion code are in fairly good agreement with those presented in Switzer & Hirata (2007a) and show that, for the interaction of photons with the considered resonances, the hypothesis of *complete redistribution* of the photons over the Voigt profile, $\phi(x)$ (see Appendix A, for definitions), is *not correct*, and may lead to significant differences, for the He I $2^1{\rm P}_1 - 1^1{\rm S}_0$ transition. However, that is not the case for the He I $2^3{\rm P}_1 - 1^1{\rm S}_0$ intercombination line, where the real dynamics is very close to the full redistribution case.

3.1. The escape probability in the He I lines

As described below, for the computations of the He II → He I spectrum in this paper, we make an ansatz about the shape of the escape probability in these lines. This hypothesis permits us to compute efficiently the escape probability in our codes without reducing the computational time significantly. This ansatz has been tested against the full results (Chluba & Sunyaev 2008, in preparation), and is found to produce accurate results for the spectrum. We first describe two particular "limiting" cases for the escape problem: the *complete redistribution* (or incoherent scattering), and the *no redistribution* case (or coherent scattering in the lab frame). The realistic case will be referred as *partial redistribution* in the line (or coherent scattering in the restframe of the atom).

For these two particular cases, we follow the procedure outlined in Switzer & Hirata (2007a), which is based on the assumption that within the range of frequencies considered around a given resonance a solution of the photon field, including resonant scattering and hydrogen continuum absorption, can be obtained under *quasi-stationary* conditions. Within ±1−10% of the line centre (or roughly $\pm10^3$−10^4 Doppler width), this approximation should be possible[4].

3.1.1. Complete redistribution (or incoherent scattering)

One finds that, in this case, the corresponding correction, $\Delta P_{\rm esc}$, to the standard Sobolev escape probability, $P_{\rm S} = [1 - {\rm e}^{-\tau_{\rm S}}]/\tau_{\rm S}$, is given by:

$$\Delta P_{\rm esc} = \int_{-\infty}^{\infty} \phi(x)\,{\rm d}x \int_{x}^{\infty} \tau_{\rm S}\,\phi(x')\,{\rm e}^{-\tau_{\rm L}(x,x')}\left[1 - {\rm e}^{-\tau_{\rm c}(x,x')}\right]{\rm d}x'. \quad (2)$$

[4] In addition, the approximation $\partial_\nu \nu N_\nu \approx \nu_0 \partial_\nu N_\nu$, where ν_0 is the transition frequency of the considered resonance and $N_\nu = I_\nu/h\nu$, demands that the solution is only considered sufficiently close to the line centre. For this reason the term connected with emission of photon due to the recombination of hydrogen (see definition of $I_{\rm C}$ in Switzer & Hirata 2007a) should be neglected, since in this process practically all photons are emitted very close to the ionization frequency $\nu_{\rm c}^{\rm H} \ll \nu_0$ of hydrogen.

Here $\tau_{\rm L}(x,x') = \tau_{\rm S}[\chi(x') - \chi(x)]$ is the optical depth with respect to line scattering off the resonance, where $\tau_{\rm S}$ is the Sobolev optical depth and $\chi(x) = \int_{-\infty}^{x} \phi(y)\,{\rm d}y$ is the normalized ($\chi(+\infty) = 1$) integral over the Voigt profile. Furthermore, we introduced the hydrogen continuum optical depth

$$\tau_{\rm c}(x,x') = \frac{c\,N^{\rm H}_{1s}}{H}\int_{\nu(x)}^{\nu(x')} \sigma^{\rm H}_{1s}(\tilde\nu)\frac{{\rm d}\tilde\nu}{\tilde\nu} \quad (3a)$$

$$\approx \frac{c\,N^{\rm H}_{1s}\sigma^{\rm H}_{1s}(\nu)}{H\,\nu} \times \frac{\nu}{3}\left[1 - \left(\frac{\nu}{\nu'}\right)^3\right], \quad (3b)$$

where $\nu(x) = \nu_0^{\rm He} + x\,\Delta\nu_{\rm D}$, $N^{\rm H}_{1s}$ is the number density of hydrogen atoms in the 1s-state, $\sigma^{\rm H}_{1s}(\nu)$ is the photoionization cross-section of the hydrogen ground state, H is the Hubble expansion factor, and $\nu_0^{\rm He}$ is the transition frequency of the helium resonance. The Doppler width, $\Delta\nu_{\rm D}$, of the line due to the motion of helium atoms is defined in Appendix A.

The computational details of the numerical integration of Eq. (2), as well as the derivation of a one-dimensional integral approximation to the full 2-dimensional integral, are discussed in Appendix B.

3.1.2. No redistribution (or coherent scattering in the lab frame)

This case corresponds to a situation in which every photon coming through the line is emitted again with the same frequency. During recombination this is a very good approximation in the very distant damping wings of the resonance. In practice, this case can be treated using the formalism described in Switzer & Hirata (2007a). For every transition $u \to l$, we need to define the quantity

$$f_{u\to l} = \frac{R^{\rm out}_{u\to l}}{A_{u\to l} + R^{\rm out}_{u\to l}} \quad (4)$$

where $R^{\rm out}_{u\to l}$ is the sum of the rates of all the possible ways of leaving the upper level but excluding the resonance, i.e. $R^{\rm out}_{u\to l} = R_{u\to c} + \sum_{i,i\neq l} R_{u\to i}$. In this equation, we have introduced the (bound-bound) rates, which are computed as

$$R_{u\to i} = \begin{cases} A_{u\to i}[1 + n_{\rm bb}(\nu_{ui})], & E_i < E_u \\ A_{i\to u}(g_i/g_{\rm u})n_{\rm bb}(\nu_{iu}), & E_i > E_u \end{cases} \quad (5)$$

and the photoionization rate, $R_{u\to c}$. This quantity, $f_{u\to l}$, gives the fractional contribution to the overall width of the upper level of all possible transitions leaving the upper level except for the resonance. In other words, $f_{u\to l}$ represents the branching fraction for absorption of a line photon to result in incoherent scattering. During helium recombination, $f_{u\to l} \sim 10^{-3}$ for the He I $2^1{\rm P}_1 - 1^1{\rm S}_0$ transition and is close to unity for He I $2^3{\rm P}_1 - 1^1{\rm S}_0$ intercombination line.

Once we have obtained this quantity for the transition, the corresponding escape probability in the case of fully coherent scattering is given by

$$P_{\rm esc} = \frac{f_{u\to l}P}{1 - (1 - f_{u\to l})P} \quad (6)$$

where

$$P = P_{\rm S}(f_{u\to l}\tau_{\rm S}) + \Delta P_{\rm esc}(f_{u\to l}\tau_{\rm S}, \tau_{\rm c}) \quad (7)$$

and where $P_{\rm S}(f_{u\to l}\tau_{\rm S})$ means that the Sobolev escape probability is evaluated at $f_{u\to l}\tau_{\rm S}$ instead of at $\tau_{\rm S}$; and obtaining $\Delta P_{\rm esc}(f_{u\to l}\tau_{\rm S}, \tau_{\rm c})$ reduces to the use of Eq. (2), but evaluating it at $f_{u\to l}\tau_{\rm S}$ instead of at $\tau_{\rm S}$, while $\tau_{\rm c}$ remains unchanged.

3.1.3. Partial redistribution case. Our ansatz

The detailed treatment of the problem with *partial redistribution* is computationally demanding. Our results are based on a diffusion code (Chluba & Sunyaev 2008, in preparation), which requires ∼1 day on a single 3 GHz processor to treat one cosmology. The other approach to this problem, based on a Monte Carlo method (Switzer & Hirata 2007a), is equally demanding.

For the computations in this paper, we propose and test an ansatz that permits us to compute the escape probability efficiently. Our basic assumption is that *the ratio of the escape probability in the complete problem (the partial redistribution case) to the escape probability in the problem with no redistribution is a constant number for a given redshift, or, equivalently, it has a very small dependence on the recombination history*. In that case, we can use this function (the ratio of the two cases) to *fudge* the real escape probability in our code very rapidly. The important thing is that we need only compute a single solution of the complete problem in order to tabulate the fudge function. Moreover, the reference case (the no redistribution case) is fully analytic, and using our 1D integral approximation described in Appendix B, it is obtained very quickly. Summarizing, this scheme permits us to compute the escape probability with high accuracy in our codes, without the need to interpolate using pre-computed tables.

In practice, we use the solution for the recombination history obtained within the no-redistribution approximation and we compute the corresponding escape probability for a given cosmology. If we make a further iteration, by recomputing the new recombination history using the new escape probability, we find that the result hardly changes. For the He I $2^3P_1 - 1^1S_0$ intercombination-line escape probability is always close to the full redistribution case, so for this line we directly consider this approximation for the computations.

3.2. Results for ΔP_{esc}

In this paper, we consider only the corrections to the escape probability for the He I $2^1P_1 - 1^1S_0$ transition and He I $2^3P_1 - 1^1S_0$ intercombination-line. In principle, all the other $n^1P_1 - 1^1S_0$ and spin-forbidden transitions are also affected by the presence of neutral hydrogen, but the effect is smaller and we omit these additional corrections for the moment.

In Fig. 3 we show different contributions to the escape probability of the two transitions, computed using different approximations as discussed in the last section. In our computations, for the He I $2^1P_1 - 1^1S_0$ transition the effect of hydrogen is starting to become important below $z \sim 2400$–2500, whereas in the case of the He I $2^3P_1 - 1^1S_0$ intercombination-line the escape probability is strongly modified only at $z \lesssim 1800$–1900. One can also clearly see, as illustrated for the complete redistribution approach, that in both cases the 1D-approximation works extremely well at nearly all relevant redshifts. In particular, the differences are small where the deviations between the inner integrand in Eq. (2), and its analytic approximation deduced from Eq. (B.3) are small (see Fig. B.1, and the discussion in Appendix B).

For the He I $2^1P_1 - 1^1S_0$ transition, the departure of the escape probability with respect to the full redistribution case is very important, being at least an order of magnitude different at redshifts below $z \approx 2200$. Moreover, the full redistribution case becomes important at earlier redshifts ($z \sim 2600$–2700), thus producing a recombination dynamics that would be much closer to the Saha solution. In other words, the assumption of complete

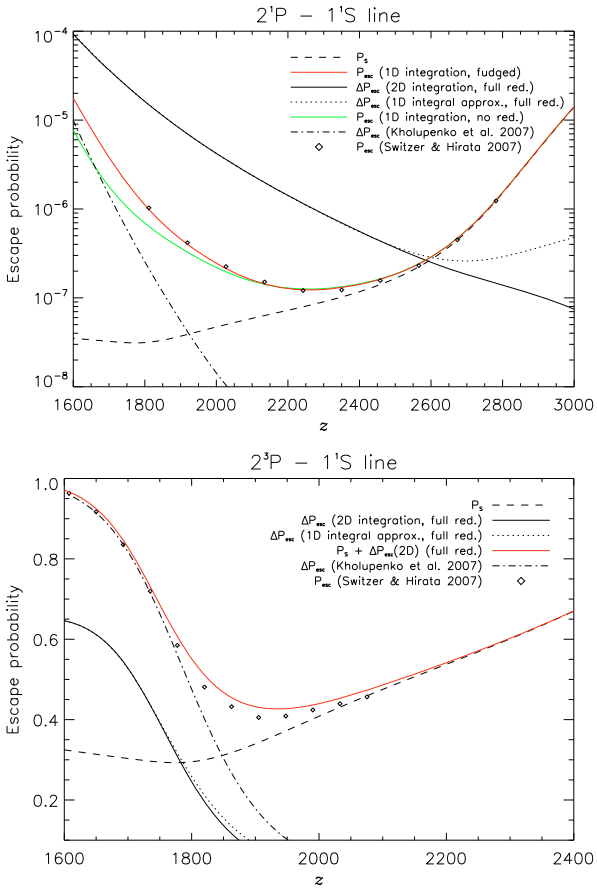

Fig. 3. Contributions to the escape probability of the He I $2^1P_1 - 1^1S_0$ transition (*upper panel*) and the He I $2^3P_1 - 1^1S_0$ intercombination-line (*lower panel*). P_S denotes the standard Sobolev escape probability. The correction to the escape probability due to the hydrogen continuum opacity is shown in several approaches. (a) Full redistribution case: the full 2D-integral, ΔP_{2D}, as given by Eq. (2), and the 1D approximation, ΔP_{1D}, obtained with Eq. (B.3); (b) no-redistribution case: the 1D approximation P_{1D}; and (c) partial redistribution case: the fudged escape probability based on the 1D integration of the no redistribution case. For comparison we show the simple analytic approximations of Kholupenko et al. (2007), and the points extracted from Fig. 11 of Switzer & Hirata (2007a) for the case labelled as coherent (which is the equivalent to our partial redistribution case) for the *upper panel*, and the points extracted from Fig. 4 of Switzer & Hirata (2007b).

redistribution significantly overestimates the escape rate of photons from the He I $2^1P_1 - 1^1S_0$ transition and would thus artificially accelerate He II → He I recombination. The final (fudged) solution is in reality much closer to the no-redistribution case, although the differences with respect to this latter case are still significant (roughly a factor of 2 at $z \sim 1730$). Comparing our results with other recent computations, we find that our final (fudged) solution is very close to the Switzer & Hirata (2007a) computation, which was based on a Monte Carlo analysis of the escape problem. There are still small differences around redshifts $z \sim 2200$–2400, which could be probably due to the fact that we do not include the modified escape for higher levels. However, the formula given in Kholupenko et al. (2007) only works at very low redshifts.

For the He I $2^3P_1 - 1^1S_0$ intercombination-transition, the situation is different. The computations, based on the diffusion code, show that for this line one can approximate the escape probability using complete redistribution at the level of ∼10%. Therefore,

for the computations in this paper, we adopt this approximation for this particular transition. The lower panel of Fig. 3 also shows the comparison between our escape probability and those obtained in other recent publications. The agreement with the Switzer & Hirata (2007a) result is again very remarkable, except for the redshift region around $z \sim 1900$. However, we have checked that this difference is mainly due to the assumption of using the full redistribution solution for this line, and that this difference implies only small changes in the final recombination spectrum. For this transition the actual corrections due to electron scattering, which we neglected so far, are larger. Finally we note that, although in this case there is an apparent agreement at low redshifts with the Kholupenko et al. (2007) result, their computation corresponds to the quantity $\Delta P_{\rm esc}$. Thus, when adding the contribution of the Sobolev escape, they have a value of the probability which exceeds unity.

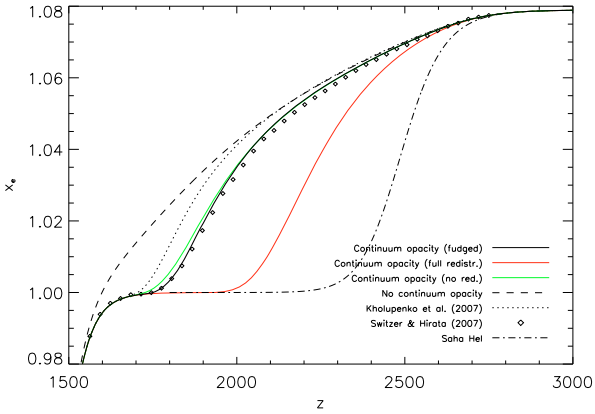

Fig. 4. The ionization history during the epoch of He II → He I recombination for different approaches.

3.3. Inclusion into the multi-level code

In order to account for the effect of the hydrogen continuum opacity during He II → He I recombination in our multi-level code several changes are necessary. The first and most obvious modification is the replacement of the Sobolev escape probability $P_{\rm S} \rightarrow P_{\rm S} + \Delta P_{\rm esc}$ for the He I $2^1{\rm P}_1 - 1^1{\rm S}_0$ and He I $2^3{\rm P}_1 - 1^1{\rm S}_0$ intercombination-transition. Because of the above replacement *more* electrons reach the ground state of neutral helium, but *no additional* helium photons are released. Therefore, in the computation of the helium spectrum the increase in the photons escape rate by $\Delta P_{\rm esc}$ should *not* be included.

Given the usual *net* radiative transition rate $P_{\rm S} \times \Delta R_{i1^1{\rm S}}$ from level i to the helium ground state, the increase in the net transition rate due to the presence of neutral hydrogen atoms is given by $\Delta R^{\rm abs}_{i1^1{\rm S}} = \Delta P_{\rm esc} \times \Delta R_{i1^1{\rm S}}$. Since the corresponding photons associated with this transition are ionizing hydrogen atoms, one has to add the rate $\Delta R^{\rm abs}_{i1^1{\rm S}}$ to the electron equation and subtract it from the hydrogen 1s-equation. Although it is clear that, given this small addition of electrons to the continuum, the hydrogen ground state population will re-adjust within a very short time, it is still possible that the corresponding electrons will reach the ground state via various decay channels, including a cascade from highly excited levels, which may even end at the 2 s level, yielding two photons in the two-photon decay transition. Instead of assuming that *all* electrons connected with the increase in the net transition rate, $\Delta R^{\rm abs}_{i1^1{\rm S}}$, lead to the emission of a hydrogen Lyman-α photon *only* (as done in Kholupenko et al. 2007), this approach is more consistent. We shall see below that some of the additional electrons indeed take more indirect routes to the hydrogen 1 s-level.

With these additions to our multi-level code it is possible to obtain both the ionization history and the helium and hydrogen recombination spectrum, including the effect of the hydrogen continuum opacity as outlined in this section.

4. The helium recombination history

The main goal of this paper is to compute the spectral distortions resulting from the bound-bound transitions of helium. However, since we are discussing several approximations to include the hydrogen absorption during the epoch of He II → He I recombination, we briefly discuss here the corresponding differences in the ionization fraction.

Figure 4 shows our results for the redshift dependence of the free electron fraction $x_{\rm e} = n_{\rm e}/n_{\rm H}$ during He II → He I recombination, using the three approximations for the escape probability in the He I lines, as discussed above. Qualitatively, all three results (i.e. full redistribution, no-redistribution and partial redistribution) agree with those found in some earlier studies (Kholupenko et al. 2007; Switzer & Hirata 2007a), showing that the inclusion of the hydrogen continuum opacity in the computation significantly speeds up recombination, making it closer to the Saha solution. Our (fudged) solution for the case of partial redistribution of photons in the resonance is in good agreement with the Switzer & Hirata (2007a), except for the small difference around $z \sim 2200$. As pointed out in the last section, these are probably due to the fact that we did not include the continuum opacity correction for higher transitions.

It is important to note that the incorrect hypothesis of full redistribution in the He I $2^1{\rm P}_1 - 1^1{\rm S}_0$-resonance has a strong impact on the recombination history. In that case, the effect of continuum opacity on the escape probability becomes of importance at earlier times, shifting the redshift at which $x_{\rm e}$ starts to depart from the solution without continuum opacity considerably. In addition, the period during which $x_{\rm e}$ is very close to unity, i.e. just before hydrogen recombination starts, becomes considerably longer. Therefore, it is very important for a detailed analysis of the recombination history to treat properly the escape probability in this line.

So far we have not considered the effect of feedback on our computations, and as shown in Switzer & Hirata (2007a) one does expect some additional delay of He II → He I recombination around $z \sim 2400$. However, looking at Fig. 12 in Switzer & Hirata (2007a), this process is not expected to alter the results by more than 10–20%.

Finally, we also mention that for computations of the electron fraction during the epoch of He II → He I recombination, it is *not* necessary to include a very large number of shells. Unlike in the case of hydrogen recombination, the exponential tail of He II → He I recombination, which is potentially the most sensitive to the completeness of the atomic model, is entirely buried by the large number of free electrons from hydrogen. In addition, practically no ionized helium atoms remain after recombination, although in the case of hydrogen a small residual fraction remains. This is because there are significantly more electrons per helium atom than for hydrogen, such that freeze-out for helium occurs at an exponentially lower level.

Our results suggest that for He II → He I recombination the inclusion of five shells is already enough to capture the evolution of $x_{\rm e}$ during this epoch with precision better than 0.1%. This precision is sufficient if one is interested in cosmological parameter

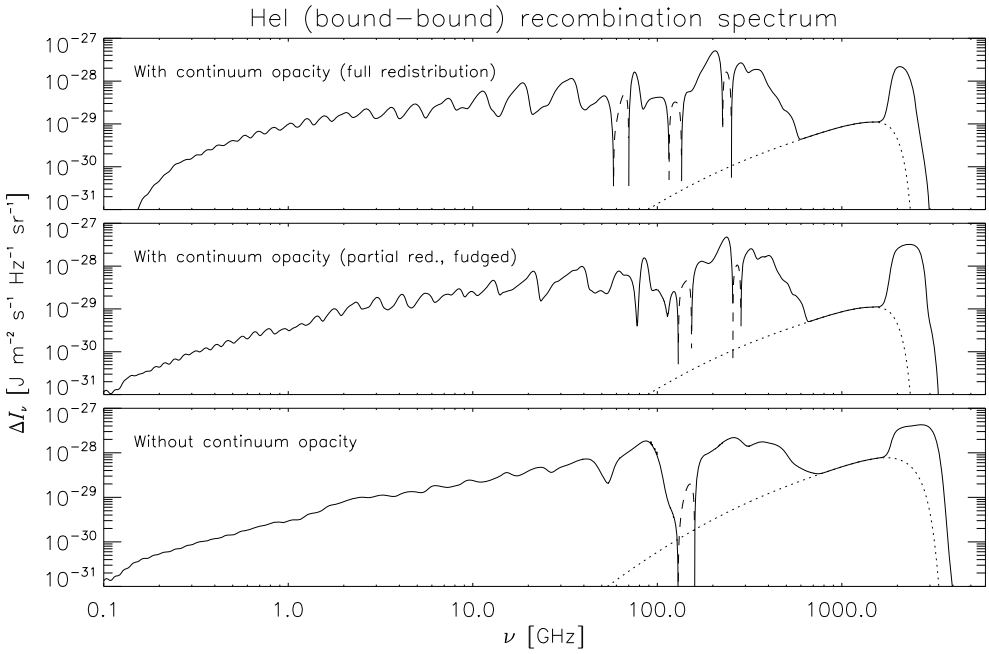

Fig. 5. A comparison of the He I recombination spectrum for $n_{\rm max} = 30$ with (*top and middle panels*) and without (*bottom panel*) inclusion of the effect of hydrogen continuum opacity. The *upper panel* corresponds to the case of full redistribution of photons in the He I $2^1P_1 - 1^1S_0$-resonance, while the *middle panel* corresponds to our final (fudged) computation for the partial redistribution case (see text for details). Ordered in this way, from top to bottom we have a progressively slower recombination, so all the features become broader. In all three cases, a solid line indicates positive values, while a dot-dashed line indicates negative ones. Two-photon decay continuum $2^1S_0 - 1^1S_0$ is also included as the dotted line in *both panels*.

estimation from the angular power spectra (C_ℓ's) of the CMB. However, still rather significant modifications of the recombination history can be expected in particular from the feedback of He II-photons and probably other physical processes that have been omitted here (for example, see Switzer & Hirata 2007a).

5. Bound-bound helium recombination spectra

In Fig. 1 we present the main result of this paper, namely the complete bound-bound helium recombination spectrum, arising both during the epoch of He III → He II ($5000 \lesssim z \lesssim 7000$), and He II → He I recombination ($1600 \lesssim z \lesssim 3000$). For comparison, we have also included the results obtained in our previous computations for the H I bound-bound recombination (Chluba et al. 2007) and have added the additional lines appearing as a consequence of the re-processing of He I photons in the continuum of hydrogen, as described below (see Sect. 5.2). Also, the 2 s two-photon decay continua for all cases are shown. There are two important issues to be mentioned here:

(i) First, the helium spectral features (both for He II and He I) are significantly narrower than those of the hydrogen recombination spectrum. This is because for He I, recombination occurs significantly faster due to the inclusion of the hydrogen continuum opacity, and in the case of He II because its recombination occurs much more close to Saha conditions in the first place. Even the inclusion of Doppler broadening due to electron scattering, as described in Sect. 5.5, is unable to change this aspect. As a consequence, both recombination spectra contain clear features in the low frequency domain ($\nu \sim 1$ GHz), where the H I spectrum is practically featureless. This increase in the amplitude of variability of the recombination radiation at low frequencies might help to detect these features in the future.

(ii) The He I recombination spectrum displays *two negative features*, at $\nu \approx 145$ and 270 GHz. This is qualitatively different from the case of the hydrogen and He II spectra, where the net bound-bound spectra appear in emission. As we will discuss below, the reason for these features is directly connected with the dynamics of recombination. They are associated with transitions in which the lower state is effectively "blocked" for all downward transitions, such that faster channels to the 1^1S_0 level are provided through energetically higher levels.

We now discuss in detail some particular aspects of the recombination spectra.

5.1. Importance of the hydrogen continuum opacity for the bound-bound He I spectrum

In Fig. 5 we show the comparison between the He I spectrum in three cases, namely the case *with* hydrogen continuum opacity assuming full redistribution of photons in the resonance; the case *with* hydrogen continuum opacity assuming partial redistribution; and the case *without* the inclusion of the hydrogen continuum opacity in the computation.

The width of the lines, which is directly connected with the duration of the recombination process, is significantly smaller when including the effect of hydrogen continuum opacity. In addition, the peaks of the lines are shifted towards lower frequencies (i.e. higher redshifts). As a consequence, the spectrum has a richer structure as compared to the case of hydrogen, since the overlap of lines is smaller.

The full redistribution and partial redistribution spectra are very similar in the low frequency ($\nu \lesssim 30$ GHz) region. However, at higher frequencies, several differences appear. In particular, for the full redistribution computation there are *three* negative

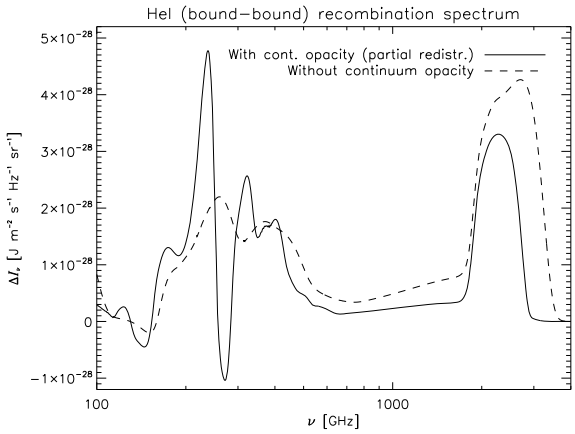

Fig. 6. A comparison of the He I recombination spectrum for $n_{\rm max} = 30$ close to the He I $2^1{\rm P}_1-1^1{\rm S}_0$ line, with (solid curve) and without (dashed curve) the effect of hydrogen continuum opacity. The case with continuum opacity corresponds to the partial redistribution (fudged) computation. The two-photon decay continuum $2^1{\rm S}_0-1^1{\rm S}_0$ is also included in the spectra.

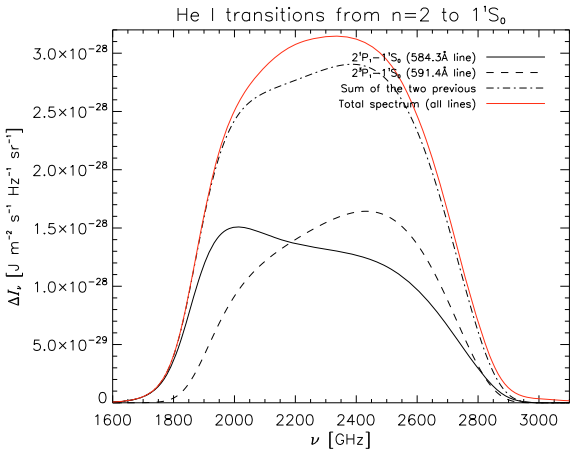

Fig. 7. Transitions in He I atom from the $n = 2$ shell to the ground state, in particular the He I $2^1{\rm P}_1-1^1{\rm S}_0$ and He I $2^3{\rm P}_1-1^1{\rm S}_0$ intercombination-lines. This figure was obtained using our results for the $n_{\rm max} = 20$ computation, including the effect of hydrogen continuum opacity in the partial redistribution case (fudged solution).

features instead of two. The spectrum for the case without continuum opacity is much smoother than the previous two and presents only *one* negative feature. In addition, in this frequency regime (and especially for the strong feature at $\nu \gtrsim 2000$ GHz) is seen that, due to the different speeds of the recombination process, the lines appear displaced towards lower frequencies (higher redshifts) as we move from the lower to the upper panel.

For the high frequency region ($\nu > 100$ GHz), we present a more detailed direct comparison in Fig. 6 between the cases of partial redistribution and the one without continuum opacity. In this figure, a linear scale in the vertical axis is used in order to emphasize the existence of the negative features. One can see that the relative contribution of the different lines is strongly altered. In general, all emission appearing above $\nu \sim 500$ GHz is suppressed, while at lower frequencies, some lines are enhanced. We can understand these changes as follows: the contributions appearing at $\nu \gtrsim 500$ GHz correspond to the $n^1{\rm P}_1-1^1{\rm S}_0$-series of neutral helium, the spin-forbidden transitions directly connecting to the ground state ($n^3{\rm P}_1 - 1^1{\rm S}_0$), and the two-photon decay of the $2^1{\rm S}_0$ singlet state. The first two series contribute most to the strong feature at $\nu \gtrsim 2000$ GHz (see Fig. 7 for some more detail), while the broad two-photon continuum dominates the spectrum in the vicinity of $\nu \sim 1000$ GHz. When the hydrogen continuum opacity is included, in our current implementation of the problem, only the He I $2^1{\rm P}_1 - 1^1{\rm S}_0$ and He I $2^3{\rm P}_1 - 1^1{\rm S}_0$ intercombination-transition are *directly* affected, i.e. via the inclusion of $\Delta P_{\rm esc}$, whereas all the other lines are modified only *indirectly* because of to the change in the *recombination dynamics* and the relative importance of different escape channels.

Figure 8 of Wong & Scott (2007) shows that without the hydrogen continuum opacity the He I $2^1{\rm P}_1 - 1^1{\rm S}_0$ channel defines the rate of recombination at $z \gtrsim 2400$, while at $z \lesssim 2400$ the $2^3{\rm P}_1 - 1^1{\rm S}_0$ spin-forbidden and, to a smaller extent, the $2^1{\rm S}_0$ two-photon decay channel dominate. Their computations show that of all electrons that reach the ground state of helium 39.9% go through the He I $2^1{\rm P}_1 - 1^1{\rm S}_0$ transition, 42.8% pass through the $2^3{\rm P}_1 - 1^1{\rm S}_0$ spin-forbidden transition and only 17.3% take the route via the $2^1{\rm S}_0$ two-photon decay channel.

In our computations including the hydrogen continuum opacity we have to keep in mind that there is a fraction of electrons that reach the helium ground state due to continuum absorption by hydrogen, which then lead to the emission of additional photons in the H I recombination spectrum. Direct integration of the total number of photons in the neutral helium spectrum around $\nu \sim 2000$ GHz yields $N_\gamma = 4\pi/c \int {\rm d}\nu \Delta I_\nu/(h\nu) \sim 0.46 N_{\rm He}$, while for the $2^1{\rm S}_0$ two-photon decay spectrum we have $\sim 0.16 N_{\rm He}$ photons. Moreover, one can compute the number of photons in the newly generated hydrogen Lyα line (see Fig. 9 below), obtaining $N_\gamma({\rm Ly}\alpha) \sim 0.44 N_{\rm He}$. These numbers show that ~90% of all electrons that reach the ground state of helium pass through the He I $2^1{\rm P}_1 - 1^1{\rm S}_0$ and He I $2^3{\rm P}_1 - 1^1{\rm S}_0$ intercombination-transition. The $2^1{\rm S}_0$ two-photon channel only allows ~8% of all helium atoms to recombine, and ~2% go through the other $n^1{\rm P}_1 - 1^1{\rm S}_0$ and $2^3{\rm P}_1 - 1^1{\rm S}_0$ spin-forbidden transitions.

We note that the modification of the dynamics of He I recombination influences the relative amplitude of other lines, such as the $3^1{\rm D} - 2^1{\rm P}$ (6680 Å) transition, which is strongly amplified, or the $3^3{\rm D} - 2^3{\rm P}$ (5877 Å) transition, which now appears in absorption. We will discuss these transitions in detail below.

To end this subsection, we recall once more that those features in the vicinity of $\nu \sim 2000$ GHz arising from the He I $2^1{\rm P}_1 - 1^1{\rm S}_0$ and He I $2^3{\rm P}_1 - 1^1{\rm S}_0$ intercombination-transitions will not be observed in the real spectrum because of feedback processes connected with HI continuum absorption at lower redshifts will take away these photons and will produce additional distortions in the HI spectrum.

5.2. Importance of the hydrogen continuum opacity for the bound-bound H I spectrum

In Fig. 8 we show how the hydrogen recombination spectrum is modified because of the additional free electrons appearing due to the absorption of He I photons in the hydrogen continuum absorption. Most of them recombine after a very short time through the main channel of hydrogen recombination at high redshifts, which is the Ly-α transition (e.g. see Fig. 10 in Rubiño-Martín et al. 2006), producing a "new" hydrogen Ly-α feature at $z \approx 1870$. In Fig. 9 we show the shape of that line separately. However, as explained in Sect. 3.3, the small addition of electrons to the continuum also produces changes in the rest of the hydrogen spectrum, as shown in Fig. 8. In some cases

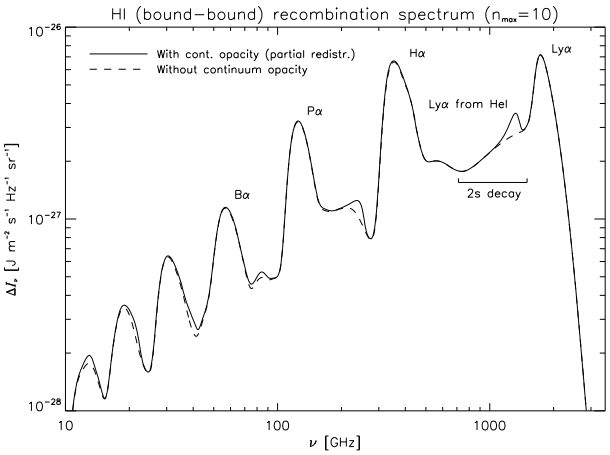

Fig. 8. A comparison of the H I recombination spectrum for $n_{\rm max} = 10$ at high frequencies, with (solid curve) and without (dashed curve) the hydrogen continuum opacity was included in the treatment of the He I atom. The 2 s two-photon decay continuum is also shown in both cases.

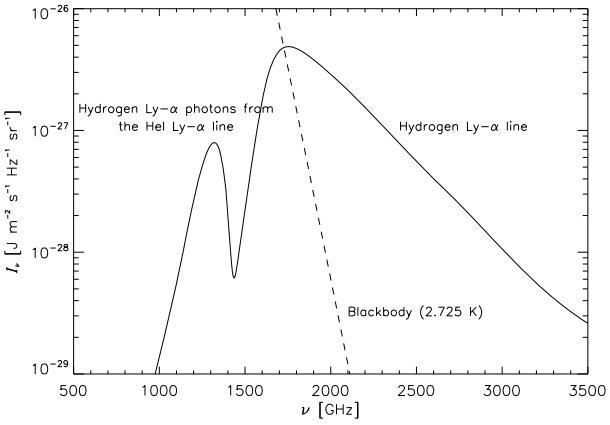

Fig. 9. Hydrogen Ly-α recombinational line. When including the effect of continuum opacity and solving simultaneously the evolution of hydrogen and helium recombination, most of the electrons which are taken from the helium by neutral hydrogen atoms reappear as a hydrogen Ly-α line at $\nu \approx 1320$ GHz ($z \approx 1870$).

(e.g. the high-frequency wing of the Paschen series) the changes are important at the 10 percent level. This feature is due to the new Hα feature. On average, the new bound-bound H I spectrum is slightly higher in amplitude, as a consequence of the additional photons appearing in this process. Because the reprocessing of He I photons occurs at high redshifts (above $z = 1800$), the two-photon continuum line is practically unchanged.

5.3. Negative features in the He I spectrum

One of the most interesting results of our computations is the existence of two *negative* features in the He I recombination spectrum. In order to identify the transitions that contribute most to those features, in Table 1 we provide a list with the position and amplitudes of all the individual lines which are found to be negative at an amplitude smaller than -1×10^{-29} J m^{-2} s^{-1} Hz^{-1} sr^{-1} from our $n_{\rm max} = 20$ computation. To help in the discussion, we also provide in Table 2 a list with the position and amplitudes of all the *positive* individual lines which are found to have an amplitude larger than 1×10^{-29} J m^{-2} s^{-1} Hz^{-1} sr^{-1} from the same computation.

Table 1. Positions and amplitudes of all the negative lines in the He I recombination spectrum for $n_{\rm max} = 20$ with peak intensities smaller than -1×10^{-29} J m^{-2} s^{-1} Hz^{-1} sr^{-1}. We show the corresponding terms for the lower and upper states, the peak intensity at the minimum, the central frequency (ν_0) as observed today, the redshift ($z_{\rm min}$) at the minimum, and the wavelength for that transition in the rest frame ($\lambda_{\rm rest}$).

Lower	Upper	ΔI_ν at minimum [J m^{-2} s^{-1} Hz^{-1} sr^{-1}]	ν_0 [GHz]	$z_{\rm min}$	$\lambda_{\rm rest}$ [Å]
2^1S_0	2^1P_1	-1.1×10^{-28}	78	1855	20 590
3^3D_2	4^1F_3	-1.1×10^{-28}	86	1875	18 690
3^3D_3	4^1F_3	-1.5×10^{-29}	86	1875	18 690
3^3D_2	5^1F_3	-1.2×10^{-29}	125	1875	12 790
4^3D_2	5^1F_3	-1.2×10^{-29}	40	1875	40 380
2^3S_1	2^3P_1	-2.1×10^{-28}	145	1905	10 830
2^3P_1	3^3D_2	-1.6×10^{-28}	273	1870	5877
2^3P_2	3^3D_2	-5.9×10^{-29}	272	1875	5877
3^3D_2	4^3F_3	-1.0×10^{-28}	86	1870	18 690
3^3D_3	4^3F_3	-1.4×10^{-29}	86	1875	18 690
4^3D_2	5^3F_3	-1.1×10^{-29}	40	1875	40 380

Table 2. Positions and amplitudes of all the positive lines in the He I recombination spectrum for $n_{\rm max} = 20$ with peak intensities greater than 2×10^{-29} J m^{-2} s^{-1} Hz^{-1} sr^{-1}. We show the corresponding terms for the lower and upper states, the peak intensity at maximum, the central frequency ν_0 as observed today, and the wavelength for that transition in the rest frame ($\lambda_{\rm rest}$).

Lower	Upper	ΔI_ν at maximum [J m^{-2} s^{-1} Hz^{-1} sr^{-1}]	ν_0 [GHz]	$z_{\rm max}$	$\lambda_{\rm rest}$ [Å]
1^1S_0	2^1P_1	1.5×10^{-28}	2011	2550	584.3
1^1S_0	2^3P_1	1.6×10^{-28}	2430	2085	591.4
2^1S_0	3^1P_1	7.5×10^{-29}	317	1885	5017
2^1S_0	4^1P_1	2.2×10^{-29}	401	1885	3966
2^1P_1	3^1S_0	2.4×10^{-29}	218	1885	7283
2^1P_1	3^1D_2	4.6×10^{-28}	239	1880	6680
2^1P_1	4^1D_2	8.0×10^{-29}	323	1885	4923
2^1P_1	5^1D_2	3.0×10^{-29}	362	1885	4389
3^1D_2	4^1F_3	1.7×10^{-28}	85	1875	18 700
3^1D_2	5^1F_3	3.1×10^{-29}	125	1880	12 790
3^1D_2	4^3F_3	1.5×10^{-28}	85	1875	18 700
3^1D_2	5^3F_3	2.1×10^{-29}	125	1880	12 790
4^1D_2	5^1F_3	2.4×10^{-29}	39	1880	40 410
4^1F_3	5^1G_4	2.3×10^{-29}	39	1885	40 490
2^3S_1	2^3P_0	3.2×10^{-29}	146	1890	10 830
2^3S_1	2^3P_2	8.4×10^{-29}	142	1950	10 830
2^3S_1	3^3P_2	2.5×10^{-29}	408	1890	3890

We now discuss in detail each one of these two negative features. Figures 10 and 11 present them separately, together with the main contributors according to the list of transitions in Tables 1 and 2. For completeness, we also discuss in this subsection the feature which is associated with the $2^1S_0 \rightarrow 2^1P_1$ singlet-singlet transition. Figure 12 shows the contribution of this line to the total spectrum in that region. Although this particular line is negative, the overall spectrum in the region is positive due to the added contribution of other lines.

5.3.1. First negative feature ($\nu \approx 145$ GHz)

As Fig. 10 indicates, the largest negative contribution comes from one of the 10 830 Å fine-structure lines. The appearance of this feature in absorption can be understand as follows. The channel connecting the 2^3S_1 triplet level with the singlet ground

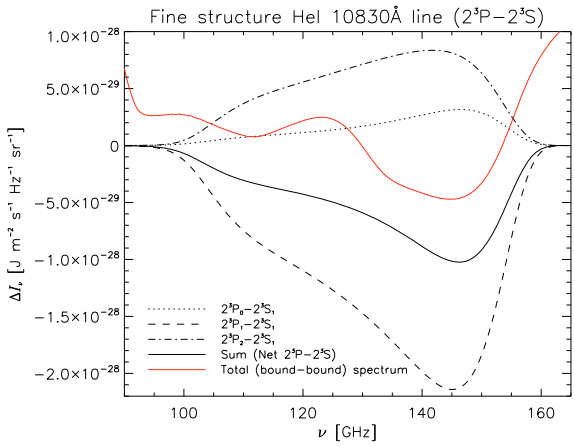

Fig. 10. First negative feature in the He I spectrum. The largest negative contribution comes from the 10 830 Å fine-structure line. Note that the upper level has fine structure, so we present all three possible values of J. This figure was obtained using our results for the $n_{\rm max} = 20$ computation, including the effect of hydrogen continuum opacity.

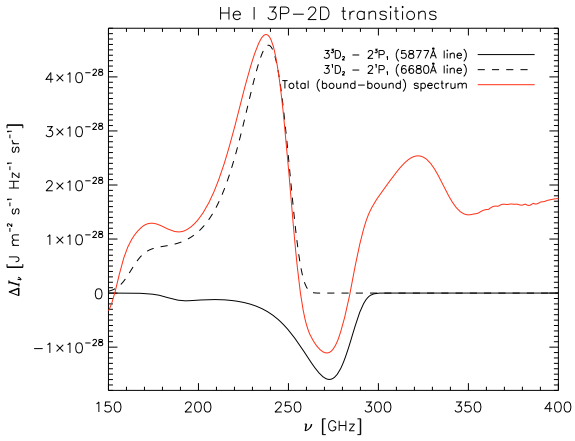

Fig. 11. Second negative feature in the HeI spectrum. The largest negative contribution is produced by the 3D–2P (triplet-triplet) transition. This figure was obtained using our results for the $n_{\rm max} = 20$ computation, including the effect of hydrogen continuum opacity.

state via the two-photon decay is extremely slow ($\sim 4\times10^{-9}$ s^{-1}) and therefore renders this transition a "bottleneck" for those electrons recombining through the 2^3S_1 triplet state. Since the electrons in the 2^3P_1 triplet level can reach the 1^1S_0 level via the much faster ($\sim$177 s^{-1}) He I $2^3P_1 - 1^1S_0$ intercombination-transition, this provides a more viable route. On the other hand the 2^3P_0 and 2^3P_2 do not have a direct path to the singlet ground state. But as one can see from Table 2 this restriction can be avoided by taking the route $2^3P_{0/2} \rightarrow 2^3S_1 \rightarrow 2^3P_1 \rightarrow 1^1S_0$. The relative amplitude of these lines seen in Fig. 10 also suggests this interpretation.

5.3.2. Second negative feature ($\nu \approx 270$ GHz)

The second overall negative feature in the bound-bound He I recombination spectrum is mainly due to the superposition of the negative 5877 Å and positive 6680 Å-lines (see Fig. 11). Here, it is interesting that in Table 2 no strong positive triplet-singlet transition appear, which actually starts with a 3^3D_2-state. However, Table 1 shows a strong flow from the 3^3D_2-state to higher F-level exists, again permitting electrons to pass to the

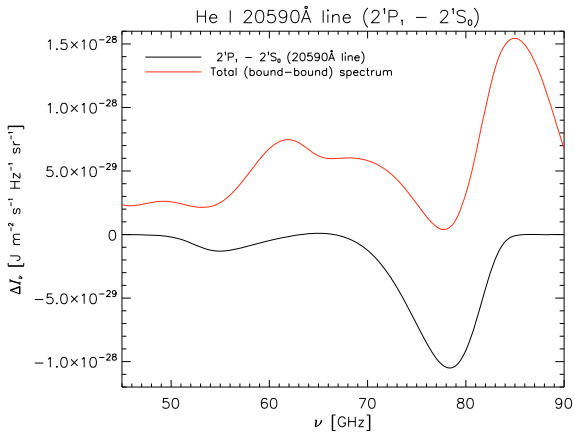

Fig. 12. The He I recombination spectrum in the vicinity of the 20 590 Å line. This figure was obtained using our results for the $n_{\rm max} = 20$ computation, including the effect of hydrogen continuum opacity.

singlet-ground level because of singlet-triplet mixing. This then also contributes to the nearby emission feature via the chain $2^3P_1 \rightarrow 3^3D_2 \rightarrow 4^3F_3 \rightarrow 3^1D_2 \rightarrow 2^1P_1$.

5.3.3. The spectrum in the vicinity of $\nu \approx 80$ GHz

Figure 12 shows that in this spectral region, there is a clear low-intensity feature in the overall spectrum, which is produced by the $2^1S_0 \rightarrow 2^1P_1$ singlet-singlet transition, which contributes as a negative line. Comparing the 2^1S_0 two-photon decay rate ($A_{2^1S_0-1^1S_0}$) with the transition rate to the 2^1P_1, shows that at $z \sim 2500$ the latter is a factor of 2×10^4 larger. Therefore, whenever escape in the He I $2^1P_1 - 1^1S_0$ line substantially controls the rate of helium recombination, the $2^1S_0 \rightarrow 2^1P_1$ singlet-singlet transition appears in absorption. As explained above, in accounting for the hydrogen continuum absorption this is the case at all redshifts of importance.

However, the situation is a bit more involved, since several other transitions contribute to the negative ($3^3D_2 \rightarrow 4^1F_3$, $3^3D_3 \rightarrow 4^1F_3$, $3^3D_2 \rightarrow 4^3F_3$ and $3^3D_3 \rightarrow 4^3F_3$) and positive ($4^1F_3 \rightarrow 3^1D_2$ and $4^3F_3 \rightarrow 3^1D_2$) centred at $\nu \approx 85$ GHz. The superposition of these lines then yields an oscillatory feature between 80 and 90 GHz, which although always positive, still shows the clear signature from the 20 590 Å line. Here it is important to realize that several triplet-singlet transitions are involved, allowing triplet atoms to decay further to the singlet ground state. This emphasizes the importance singlet-triplet mixing for the spectrum, and in particular well-mixed levels like the low nF-states and beyond (mixing angle $\sim$45°, see Table 11.12 in Drake 1996) provide very attractive routes.

5.4. The He II-recombination spectrum

The recombination history of He III is the one which is most close to the Saha solution (e.g. see Fig. 15 in Switzer & Hirata 2007b). The release of photons therefore occurs during a shorter period than in the case of H II and He II recombination. In comparison to hydrogen, the release of He III recombination photon happens at a redshift and temperature roughly four times higher (roughly 1400 for hydrogen as compared with 6000 for He III).

As Fig. 1 shows, the high-frequency feature always appears in the red wing of the corresponding hydrogen lines. However, at low frequencies the oscillatory feature drops out of phase with

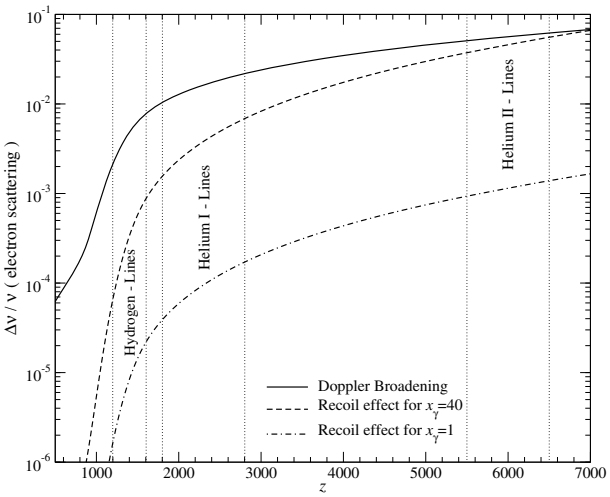

Fig. 13. Influence of electron scattering on an initially narrow line for different emission redshifts. The vertical lines indicate the epochs of recombination at which most of the photons are emitted.

the hydrogen lines. It is also interesting to see that the He II and He I bound-bound spectra show *constructive* (at $\nu \geq 10\,\mathrm{GHz}$) and also *destructive* ($\nu \sim 2{-}5\,\mathrm{GHz}$) interference. As mentioned above, this fact strongly increases the probability of observing these features in the future.

5.5. Changes in the spectra due to electron scattering

The procedure to include approximately the effects of photon scattering off free electrons is outlined in the Appendix C. However, here we neglect the corrections to the recombination history and recombination spectra arising from changes in the escape of photons from the optically thick resonances, but these are expected to be rather small.

In Fig. 13 we show the comparison of the Doppler broadening and recoil term for different redshifts. During the epoch of hydrogen recombination Doppler broadening is less than 1%, while it exceeds ∼2% during He II → He I recombination and reaches ∼7% at the beginning of He III → He II recombination. We also show the strength of the recoil term for $x_\gamma = 1$ and $x_\gamma = 40$. The latter case provides an estimate for the equivalent of the Lyman-α line of the corresponding atomic species. One can see that during hydrogen recombination the recoil term is completely negligible. During He II → He I recombination the He I $2^1\mathrm{P}_1 - 1^1\mathrm{S}_0$ line is shifted by $\lesssim$1% and only for the He II Ly-α Line is the recoil shift comparable with the broadening due to the Doppler term. We shall therefore neglect the recoil term for the hydrogen and He II → He I recombination spectrum.

Figure 14 shows the importance of the Doppler and recoil term for the He III → He II bound-bound recombination spectrum. At low frequencies Doppler broadening strongly lowers the contrast of the quasi-periodic intensity pattern, while, as expected, the recoil term is unimportant at there. Similarly, the high-frequency features are slightly smoothed out due to the Doppler effect, but the recoil term only becomes important for the He II Lyman and Balmer series photons. However, since in this work we have not yet included the reprocessing of He II photons in the continuum of He I or the feedback absorption by hydrogen, we shall not consider the corrections to the He III recombination spectrum due to the recoil term any further. A more complete treatment of this problem will be left for future work. Also, given the overall uncertainty in our model of the neutral

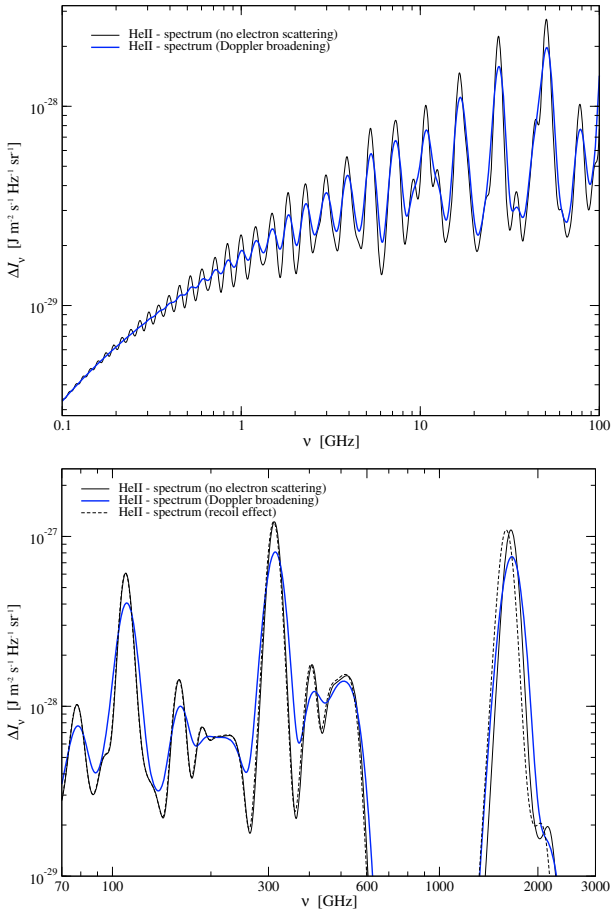

Fig. 14. Influence of electron scattering on the He III → He II bound-bound recombination spectrum. The upper panel shows the changes at low frequencies, where recoil is negligible. The lower panel illustrates the importance of the recoil term for the He II Lyman and Balmer series.

helium atom we have not included the effect of Doppler broadening for the He II recombination spectrum.

6. Discussion

In this section we now critically discuss the results presented in this paper for the helium recombination spectrum. We expect that an overall ∼10−30% uncertainty is associated with our modelling of neutral helium, while neglected physical processes are expected to lead to a modification of the resulting bound-bound helium spectra by ∼10−20%.

We would like to mention that, in addition to the aspects discussed below, another ∼30−40% rather smooth contribution to the total recombination emission can be expected from the free-bound components of hydrogen (Chluba & Sunyaev 2006a) and helium, possibly with stronger signatures at high frequencies.

6.1. Uncertainties in our modelling of the helium atom

6.1.1. Completeness of the atomic model

Probably the largest uncertainty is connected with our model of neutral helium. First of all, for our final bound-bound He I spectrum (see Fig. 1) we included only levels with $n \leq 30$. As is known from computation of the hydrogen recombination spectrum (Rubiño-Martín et al. 2006; Chluba & Sunyaev 2006a; Chluba et al. 2007), at low frequencies the level of emission

strongly depends on the completeness of the atomic model. We therefore expect rather significant modifications of the He I spectrum at frequencies below a few GHz. Computations including up to 100 shells or more are probably necessary. In the case of the bound-bound He II spectrum, for which we already included l-resolved 100 shells, the results are probably converged with similar accuracy as the one for hydrogen (see Chluba et al. 2007 for discussion).

Neither have we considered quadrupole transitions in our computations. However, from the typical values of the oscillator strengths (e.g. Cann & Thakkar 2002), one would expect that their inclusion should produce small changes.

6.1.2. Photoionization cross-sections

The next large uncertainty is due to the use of rescaled hydrogenic approximations for the high-n photoionization cross-sections. We expect differences at a level of 10−20% due to these. Here in particular, the exact frequency dependence of the cross-section may influence the importance of stimulated recombinations, which become important for excited levels. Even for $n = 5$ there are notable differences when using hydrogenic formulae instead of the fits by Smits (1996) and Benjamin et al. (1999). Moreover, we find typical differences of the order of 5−10% (and in some lines 20%) between these fits and the photoionization cross-sections obtained from the TOPbase database (Cunto et al. 1993).

Furthermore, as shown in Fig. 1 of Chluba et al. (2007) for hydrogen, due to the strong dependence of the Gaunt factor on l, for large n most of the recombinations actually go via levels with small l. In particular the S and P states of neutral helium should still have significant non-hydrogenic contribution for $n > 10$, which we did not account for in our model, again yielding a rather large uncertainty for He II $\rightarrow$ He I recombination. Due to the full hydrogenic character for the wave functions of the He II atom, there is no significant uncertainty due to the cross-sections for He III $\rightarrow$ He II recombination.

6.1.3. Energies and transition rates

In terms of level energies and transition rates, our model of the neutral helium atom is probably accurate to a level of 1−10%. The main uncertainty is connected with the neglect of singlet-triplet mixing for $n > 10$. As Table 11.12 in Drake (1996) shows, for $n = 10$ the P and D states are still nearly orthogonal, while the F states are reasonably mixed, and mixing is practically complete for all the other levels. However, there are reasons why this may not be of such extreme importance: the highly excited levels ($n \geq 10$) are already very close to the continuum. Therefore, the route via the continuum leads to a quasi-mixing of the high levels. In addition, the cascade of electrons to lower levels, where mixing is fully included, is very fast, such that no significant blocking of electrons in the higher levels is expected. However, the emission of low frequency photons probably will be underestimated. Here, a more rigorous analysis is required.

6.2. Additional physics missing in our computation

6.2.1. H I continuum opacity

As discussed in Sect. 3, the hypothesis of *complete redistribution* is not valid for the He I $2^1P_1 - 1^1S_0$ line. This assumption was usually very good in the context of hydrogen lines (Grachev 1989; Rybicki & dell'Antonio 1994), in particular due to the presence of a huge amount of CMB blackbody photons, which allow electrons to pass to higher levels while they are undergoing a resonant scattering event. However, that is not the case here because of the additional continuum opacity due to small traces of neutral hydrogen during helium recombination.

To efficiently compute the escape probability in the He I $2^1P_1 - 1^1S_0$ line, we make an ansatz of its redshift dependence. This means that we fudge the *no redistribution* solution to the escape probability with a certain factor which is obtained from a diffusion code which treats in detail the escape problem. Although this simplification may introduce errors in the frequency spectrum of a few percent, we consider this acceptable given the uncertainty in the atomic model and the photoionization cross-sections.

We also made the simplification of assuming the validity of *complete redistribution* for the He I $2^3P_1 - 1^1S_0$ intercombination line. The exact treatment of the escape of photons in this line may also lead to differences of ten percent in the spectrum. In agreement with Switzer & Hirata (2007b), our more detailed computations (Chluba et al. 2008, in preparation) show that here electron scattering plays an interesting role.

Finally, we stress that in this paper, we considered only the detailed computation of the deviations of the escape probability with respect to the Sobolev approximation for the He I $2^1P_1 - 1^1S_0$ transition and He I $2^3P_1 - 1^1S_0$ intercombination line. Inclusion of all the other $n^1P_1 - 1^1S_0$ and spin-forbidden transitions may lead to corrections of the order of 10% as well.

6.2.2. He I continuum opacity

The absorption of He II Lyman-α photons by the small fraction of neutral helium atoms during He III $\rightarrow$ He II recombination will lead to the appearance of additional He I photons, just as in the case of hydrogen (see Sect. 5.2). But since the number of photons emitted in the He II Lyman-α line is comparable to the total number of helium nuclei, this will be a notable change. Most obviously, the He II Lyman-α line will nearly disappear. In addition this will accelerate He III $\rightarrow$ He II recombination, bringing it even closer to the Saha solution.

6.2.3. Feedback processes

As mentioned in Sect. 4, for He II $\rightarrow$ He I-recombination probably one of the most important processes that we neglected in our computations so far is *feedback*. As we have seen in Sect. 5 (e.g. Fig. 7), the total number of photons emitted in the He I $2^1P_1 - 1^1S_0$ transition is comparable with those coming from the spin-forbidden $2^3P_1 \rightarrow 1^1S_0$ line.

The former has an energy that is higher by $\Delta\nu/\nu \sim 1\%$. One therefore expects the He I $2^1P_1 - 1^1S_0$ photons to interact with the He I $2^3P_1 - 1^1S_0$ intercombination resonance after a very short period of redshifting. The maximum of the He I $2^1P_1 - 1^1S_0$ line appears at $z \sim 2550$ (see Table 2), such that the bulk of these photons reach the spin-forbidden transition at $z_f \sim 2520$. At this redshift the optical depth in the spin-forbidden line is $\lesssim 1$, so that this feedback will not be complete. Still one should check this process more carefully.

As mentioned above, there is some *pure* continuum absorption, far from the resonances where resonance scattering can be neglected, that is not included into our program. This process should also lead to the reprocessing of the remaining He I $2^1P_1 - 1^1S_0$ and He II Lyman-α photons, such that in practical terms *only* the hydrogen Lyman-α line will survive at the end,

but potentially with interesting traces of the recombination history from earlier epochs. Also, the feedback due to photons emitted in the He I $n^1P_1 - 1^1S_0$ series (see Switzer & Hirata 2007a; and also Chluba & Sunyaev 2007a, for more detail) and similarly for He II, should lead to some modifications. However, these are expected to be rather small.

6.2.4. Two-photon decays

The simplest addition to the two-photon processes is the inclusion of *stimulated emission*, as suggested earlier for hydrogen (Chluba & Sunyaev 2006b) and also included by Hirata & Switzer (2007) for helium. These should modify the 2 s two-photon continua at the few percent level. However, we have shown that when accounting for the effect of hydrogen continuum absorption on He II $\rightarrow$ He I recombination, only 8% of all helium atoms reach the ground state via this channel. Hence, one does not expect large changes in the He I recombination spectrum.

For the epoch of He III $\rightarrow$ He II recombination this may be somewhat different, since electrons in higher levels will feel the change in the support of the levels from below, because at that time the two-photon decay channel is more important. In our computations ~44% of all electrons reach the ground state of He II via the two-photon channel, and the rest pass trough the He II Lyman-series. In addition one should include the reabsorption of escaped helium Lyman-α photons by the two-photon process as discussed by Kholupenko & Ivanchik (2006) for the case of hydrogen.

Also, one could think about the two-photon decays from higher levels (Switzer & Hirata 2007a; Chluba & Sunyaev 2007c) but, both in terms of additional photons and the increase in the overall rate of recombination, one expects corrections at a level of less than 1%.

6.2.5. Collisional processes

In the computations for this paper, collisional processes have not been taken into account. As discussed in Chluba et al. (2007) for the case of the hydrogen recombination spectrum, because of the large entropy of the Universe, collisional processes only modify the populations of the hydrogen levels for very high shells. In that paper it is shown that l-changing collisions need to be included only for shells above $n \gtrsim 30$–40, while n-changing collisions can be neglected even for shells as high as $n \approx 100$.

In the case of helium recombination, the same qualitative behaviour is expected. Although in this case there are more electrons and protons per helium atom than in the case of hydrogen, we still expect a small effect from collisions, that would mainly affect the high-n shells, i.e. it would only have an impact on the low-frequency tail of the recombination spectrum presented in Fig. 1. A detailed consideration of the importance of collisions on the results will be left for a future article.

7. Conclusion

We have presented detailed computations of the contributions to the cosmological recombination spectrum due to bound-bound transitions in primordial helium. The reprocessing of He I $2^1P_1 - 1^1S_0$ and He I $2^3P_1 - 1^1S_0$ intercombination photons by neutral hydrogen has been taken into account, yielding a significant acceleration of He II $\rightarrow$ He I and hence much more narrow features than without the inclusion of this process. In addition,

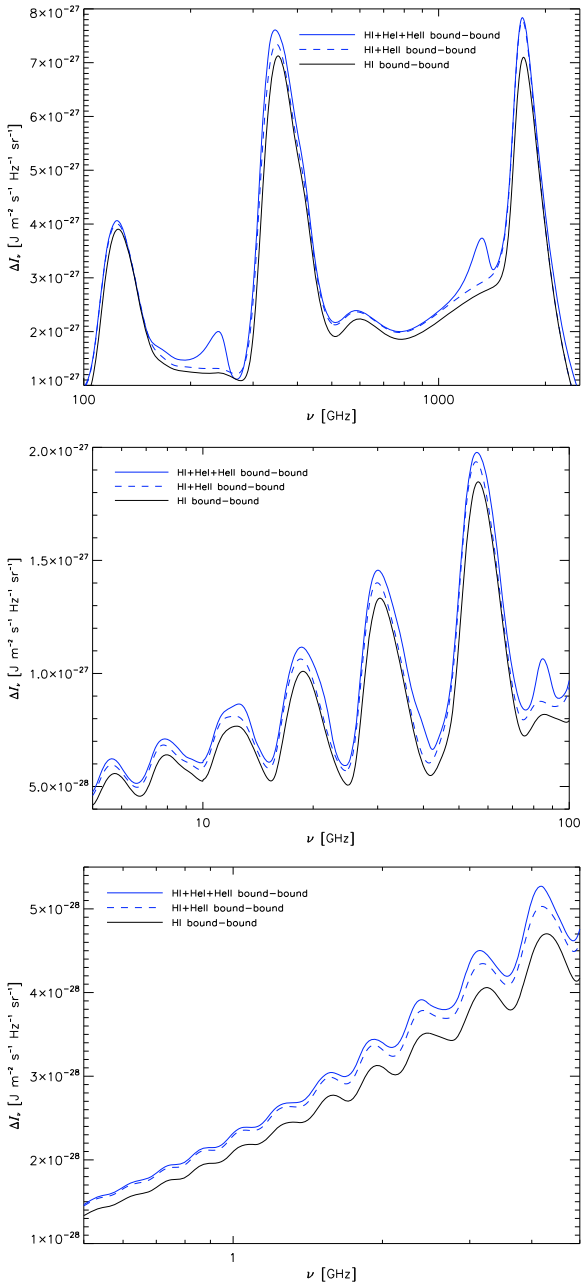

Fig. 15. Relative contribution of the H I , He I and He II bound-bound recombination spectra to the total spectrum at high- (*top*), intermediate- (*middle*) and low- frequencies (*bottom*). Helium recombination spectra (both He I and He II) modify the shapes of the existing hydrogen features, shift the peaks positions and introduce new features that represent changes of 30–40% with respect to the H I recombination spectrum alone.

some hydrogen photons are released prior to the actual epoch of hydrogen recombination at $z \sim 1100$–1500, with distinct traces due to the hydrogen Ly-α transition (see Fig. 1).

Probably the most interesting result is the presence of two negative features in the He II $\rightarrow$ He I recombinational spectrum. This is qualitatively different from any of the other spectra discussed so far (H I and He II). One of those negative features is associated with fine-structure transitions in neutral helium.

As illustrated in Fig. 1, the *total* cosmological recombination spectrum contains non-trivial signatures of all recombination epochs. We emphasize this fact in Fig. 15, where we present

a detailed view, using linear intensity scale, of three regions in the recombination spectrum covering the low, intermediate and high frequency domain. Although the relative number of helium to hydrogen nuclei is rather small (~8%), constructive and destructive interference of the oscillatory emission patterns at low frequencies, and strong non-overlapping lines at high frequencies may provide a unique opportunity to determine some of the key cosmological parameters, and to confront our current picture of recombination with experimental evidence. Interestingly, the signatures due to helium may allow direct determination of its relative abundance, much before the first appearance of stars, and as pointed out in Sunyaev & Chluba (2007), these measurements do not suffer from limitations set by cosmic variance.

As we outlined in Sect. 6, several neglected processes have to be studied in connection with helium recombination, in order to obtain definite predictions, possibly with additional revisions. Nevertheless, all the results presented here depend strongly on our understanding of atomic physics *and* the processes in the early Universe. Currently in particular the data for neutral helium may still not be sufficient. Here, help from atomic physicist is required in order to increase the availability of more complete *accurate* and *user-friendly* atomic data, in particular for the photoionization cross-sections and transition rates.

All the numerical predictions for the recombination lines obtained in this paper used to produce all the figures can be downloaded from `http://www.iac.es/galeria/jalberto/recomb`.

Acknowledgements. The authors thank I.L. Beigman and L.A. Vainshtein for many useful discussions on the physics of neutral helium, and R. Porter for useful discussions on details of the paper by Bauman et al. (2005).
We also acknowledge use of the CUBA-Library (Hahn 2004).

Appendix A: Voigt profile

Evaluations involving the well-known *Voigt* profile (e.g. see Mihalas 1978):

$$\varphi(\nu) = \frac{a}{\pi^{3/2}\,\Delta\nu_{\rm D}} \int_{-\infty}^{\infty} \frac{{\rm e}^{-t^2}\,{\rm d}t}{a^2+(x-t)^2} = \frac{\phi(\nu)}{\Delta\nu_{\rm D}}, \tag{A.1a}$$

are usually extremely time-consuming. However, convenient approximations can be given in the very distant wings and also close to the centre of the line. In Eq. (A.1a) $x = \frac{\nu-\nu_0}{\Delta\nu_{\rm D}}$ denotes the dimensionless frequency variable, and the Voigt parameter and Doppler width of the line are defined by

$$a = \frac{A_{21}}{4\pi\Delta\nu_{\rm D}} \overset{^2{\rm P}_1-{}^1{\rm S}_0}{\approx} 1.6\times10^{-3}\left[\frac{(1+z)}{2500}\right]^{-1/2} \tag{A.1b}$$

$$\frac{\Delta\nu_{\rm D}}{\nu_0} = \sqrt{\frac{2kT_{\rm e}}{m_{\rm He}c^2}} \approx 1.7\times10^{-5}\left[\frac{(1+z)}{2500}\right]^{1/2}, \tag{A.1c}$$

respectively. Here ν_0 is the transition frequency and A_{21} the Einstein coefficient for spontaneous emission for the considered resonance. $m_{\rm He} \approx 4m_{\rm p}$ is the mass of the helium atom. Note that for the spin-forbidden $2^3{\rm P}_1 - 1^1{\rm S}_0$ transition the Voigt parameter is ~170 times smaller than for the He I $2^1{\rm P}_1 - 1^1{\rm S}_0$ transition.

For $|x| \leq 30$ we use the approximation based on the Dawson integral up to sixth order as described in Mihalas (1978, Sect. 9.2, p. 279). In the distant wings of the line ($|x| \geq 30$) we apply the Taylor expansion

$$\phi_{\rm wings} \approx \frac{a}{\pi x^2}\left[1+\frac{3-2a^2}{2x^2}+\frac{15-20a^2}{4x^4}+\frac{105(1-2a^2)}{8x^6}\right]. \tag{A.2}$$

For the He I $2^1{\rm P}_1-1^1{\rm S}_0$ and spin-forbidden $2^3{\rm P}_1-1^1{\rm S}_0$ transition we checked that the Voigt function is represented with relative accuracy better than 10^{-6} over the whole range of frequencies and redshifts. Using Eq. (A.2), on the red side of the resonance one can approximate the integral $\chi = \int_{-\infty}^{x}\phi(x')\,{\rm d}x'$ by:

$$\chi_{\rm wings} = -\frac{a}{\pi x}\left[1+\frac{3-2a^2}{6x^2}+\frac{3-4a^2}{4x^4}+\frac{15(1-2a^2)}{8x^6}\right]. \tag{A.3}$$

As long as $x \lesssim -30$. Since $a \sim 10^{-3}$, this shows that in the distant wings only a very small fraction of photons is emitted. Using the symmetry of the Voigt profile one finds $\chi(x) = 1-\chi(-x)$, such that Eq. (A.3) is also applicable for $x \gtrsim 30$.

Appendix B: Computation of $\Delta P_{\rm esc}$

In this appendix, we focus on some numerical issues relevant to the evaluation of the integral in Eq. (2), which gives the escape probability in the case of complete redistribution of the photons in the resonance.

B.1. Analytical approximation of $\Delta P_{\rm esc}$

For the He I $n^1{\rm P}-1^1{\rm S}_0$ series photons $\tau_{\rm S} \gg 1$ at epochs important for helium recombination. In particular, for these one can also expect that $\tau_{\rm L} \gg \tau_{\rm c}$ at the relevant redshifts. Therefore the integrand of Eq. (2) will cut off exponentially due to the factor $\mathrm{e}^{-\tau_{\rm L}}$, while the term $1-\mathrm{e}^{-\tau_{\rm c}}$ does not change extremely fast. For the spin-forbidden transitions this condition is not fulfilled.

Using $\chi(x)$ as variable one can rewrite the integral (2) as

$$\Delta P_{\rm esc} = \int_0^1 {\rm d}\chi \int_0^{1-\chi} \tau_{\rm S}\,\mathrm{e}^{-\tau_{\rm S}\Delta\chi'}\left[1-\mathrm{e}^{-\tau_{\rm c}(\chi,\Delta\chi')}\right]{\rm d}\Delta\chi', \tag{B.1}$$

with $\Delta\chi' = \chi' - \chi$. The problem now is the computation of $\tau_{\rm c}(\chi,\Delta\chi')$. From Eq. (3b) for $[\nu'-\nu]/\nu \ll 1$ it follows

$$\tau_{\rm c}(x,x') \approx \eta_{\rm c}(\nu)[\nu'-\nu] = \eta_{\rm c}(\nu)\Delta\nu_{\rm D}[x'-x], \tag{B.2}$$

with $\eta_{\rm c} = \frac{c\,N_{\rm 1s}^{\rm H}\sigma_{\rm 1s}^{\rm H}(\nu)}{H\,\nu}$. Assuming that $\Delta x = x'-x$ is sufficiently small one may write $\Delta x \approx \Delta\chi'/\phi(x)$. It is easy to estimate that this approximation is always very good within the Doppler core, while it is rather crude in the distant wings. Inserting this into Eq. (B.1) it is possible to carry out the inner integral analytically, yielding:

$$\Delta P_{\rm esc}^{\rm 1D} \approx \int_0^1 {\rm d}\chi\left\{1-\mathrm{e}^{-\tau_{\rm S}(1-\chi)}-\kappa(\chi)\left[1-\mathrm{e}^{-[\tau_{\rm S}+\tilde\tau_{\rm c}(\chi)](1-\chi)}\right]\right\}, \tag{B.3}$$

with $\tilde\tau_{\rm c}(\chi) = \eta_{\rm c}(\nu)\,\Delta\nu_{\rm D}/\phi(x)$ and $\kappa(\chi) = \frac{\tau_{\rm S}}{\tau_{\rm S}+\tilde\tau_{\rm c}(\chi)}$, where both ν and x are functions of χ. Numerically, this integral is much easier to perform than the full 2D integral given by Eq. (2). As we will show below this approximation works very well at low redshift.

B.2. Numerical evaluation of $\Delta P_{\rm esc}$

To carry out the 2-dimension integral (2) is a cumbersome task. We used different integrators from the NAG[5] and CUBA[6]-library and only after several independent attempts finally reached agreement. It is extremely important to include the full domain of frequencies, extending the integration to the very distant

[5] See `http://www.nag.co.uk/numeric/`
[6] Download available at: `http://www.feynarts.de/cuba/`

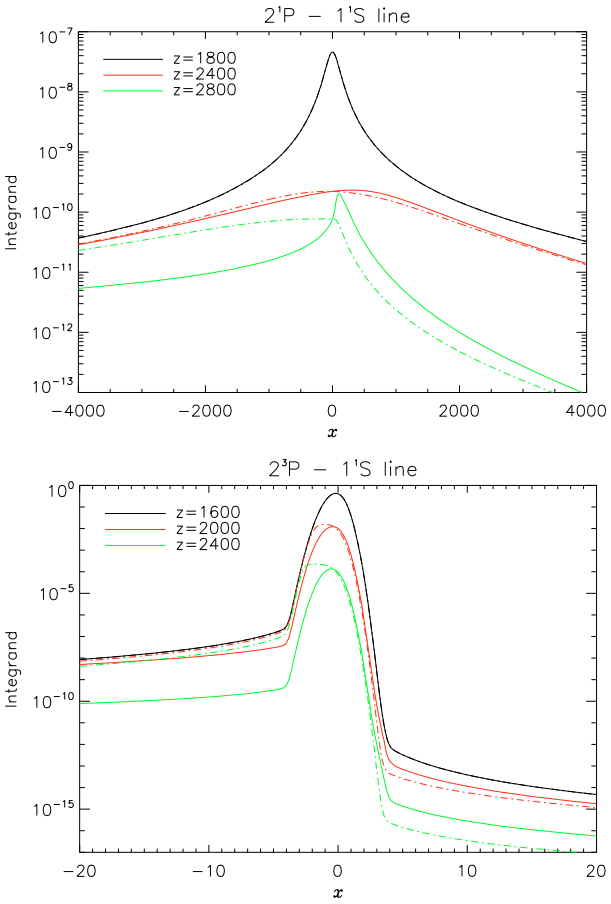

Fig. B.1. Inner integrand of $\Delta P_{\rm esc}$, as defined by Eq. (B.4), for the He I $2^1{\rm P}_1 - 1^1{\rm S}_0$ line (*upper panel*) and the spin-forbidden $2^3{\rm P}_1 - 1^1{\rm S}_0$ transition (*lower panel*). For all redshifts, the solid line corresponds to the full numerical integral, while the dot-dashed line represents the 1D approximation, as deduced from Eq. (B.3).

wings of the resonance. However, because of the extreme differences in the Sobolev escape probabilities of the He I $n^1{\rm P}_1 - 1^1{\rm S}_0$ series ($\tau_{\rm S} \sim 10^7$) and intercombination lines ($\tau_{\rm S} \sim 1$) different numerical schemes are required. In order to assure convergence of our numerical integrator we made sure that we can successfully reproduce several limiting cases for which analytical approximations can be found. In particular, we reproduced the approximation given in the previous paragraph.

In order to understand the behaviour of the integrand in Eq. (2) we define the inner integral

$$F(x) = \tau_{\rm S} \int_x^\infty \phi(x)\,\phi(x')\,{\rm e}^{-\tau_{\rm L}(x,x')}\left[1 - {\rm e}^{-\tau_{\rm c}(x,x')}\right]{\rm d}x', \qquad \text{(B.4)}$$

such that $\Delta P_{\rm esc} = \int_{-\infty}^{\infty} F(x)\,{\rm d}x$. For the He I $n^1{\rm P}_1 - 1^1{\rm S}_0$ series one always has $\tau_{\rm S} \gg 1$, such that the exponential factor ${\rm e}^{-\tau_{\rm L}(x,x')} = {\rm e}^{-\tau_{\rm S}\Delta\chi'}$ dominates the behaviour of the integrand. For a given x we numerically determined the frequency x' such that ${\rm e}^{-\tau_{\rm L}(x,x')} \leq \epsilon$, typically with $\epsilon \sim 10^{-16}$. This turned out to be rather time-consuming, but we found that even within the Doppler core a sufficient estimate for x' could be obtained using the wing expansion of the Voigt-profile, yielding the condition

$$\chi' - \chi \approx \frac{a}{\pi}\left[\frac{1}{x} - \frac{1}{x'}\right] \leq \frac{\epsilon}{\tau_{\rm S}}\,. \qquad \text{(B.5)}$$

However, here we typically chose $\epsilon \sim 10^{-25}$, in order to achieve agreement with the more rigorous treatment. For the spin-forbidden transitions this simplification is not possible, since none of the exponential factors really saturates. The full range of frequencies $x \leq x'$ had to be considered in this case. In practice we never went beyond 10^4 Doppler width.

In Fig. B.1 we show $F(x)$ for the He I $2^1{\rm P}_1 - 1^1{\rm S}_0$ line and the He I $2^3{\rm P}_1 - 1^1{\rm S}_0$ intercombination-transition. For the He I $2^1{\rm P}_1 - 1^1{\rm S}_0$ line the inner integrand becomes very broad at high redshifts, with significant contributions to $\Delta P_{\rm esc}$ out to several thousand Doppler width, while it becomes rather narrow at low redshifts. However, we found that the outer integral for $\Delta P_{\rm esc}$ nearly always has to be carried out within a very large range round the line centre. One can also see that the approximation of $F(x)$ following from Eq. (B.3) works extremely well at low redshifts. For the He I $2^3{\rm P}_1 - 1^1{\rm S}_0$ intercombination transition the main contributions to $\Delta P_{\rm esc}$ always come from within the Doppler core and the wing contribution is $\sim 10^{-8}$–10^{-7} times smaller. For the full numerical integration it is therefore possible to restrict the outer integral to a few hundred Doppler widths. In Fig. B.1 one can again see that at low redshift the approximation from Eq. (B.3) works very well.

Appendix C: Inclusion of line broadening due to electron scattering

The photons released in the process of recombination scatter repeatedly off moving electrons. In the low temperature limit this process can be described using the Kompaneets-equation. Neglecting the small difference in the photons and electron temperature at redshifts $z \lesssim 500$ and introducing the dimensionless frequency variable $x_\gamma = h\nu/kT_\gamma$, neglecting induced effects and the *recoil* term for an initially narrow line, centred at $x_{\gamma,0}$ and released at $z_{\rm em}$, one can find the solution (Zeldovich & Sunyaev 1969; Sunyaev & Titarchuk 1980)

$$\Delta I(x_\gamma, z=0)\big|_{\rm Doppler} = \frac{x_\gamma^3}{x_{\gamma,0}^3}\,\frac{\Delta I(x_{\gamma,0}, z_{\rm em})}{\sqrt{4\pi y_{\rm e}}} \times \frac{{\rm e}^{-\frac{(\ln x_\gamma + 3y_{\rm e} - \ln x_{\gamma,0})^2}{4y_{\rm e}}}}{x_{\gamma,0}}, \qquad \text{(C.1)}$$

where $\Delta I(x_{\gamma,0}, z_{\rm em})$ denotes the spectral distortion at frequency $x_{\gamma,0}$ and redshift $z_{\rm em}$ without the inclusion of electrons scattering, and the Compton y-parameter is given by

$$y_{\rm e}(z) = \int_0^z \frac{kT_{\rm e}}{m_{\rm e}c^2}\,\frac{c\,N_{\rm e}\sigma_{\rm T}}{H(z')(1+z')}\,{\rm d}z' \qquad \text{(C.2)}$$

Note that $\Delta I(x_{\gamma,0}, z_{\rm em})/x_{\gamma,0}^3 \propto \Delta n(x_{\gamma,0}, z)$, where Δn is the difference of the photon occupation number from a pure blackbody, is independent of redshift. As Eq. (C.1) shows, due to the Doppler effect, the line broadens by (compare also Pozdniakov et al. 1979)

$$\left.\frac{\Delta\nu}{\nu}\right|_{\rm Doppler} \sim 2\sqrt{y_{\rm e}\,\ln 2} \qquad \text{(C.3)}$$

and shifts towards higher frequencies by a factor ${\rm e}^{3y_{\rm e}}$.

To our knowledge no analytic solution to the Kompaneets equation that also includes the recoil term has been given in the literature. However, to estimate the effect on the spectrum one can neglect the diffusion term and finds that the line shifts by

$$\left.\frac{\Delta\nu}{\nu}\right|_{\rm recoil} \sim -y_{\rm e}\,x_{\gamma,0} \qquad \text{(C.4)}$$

towards lower frequencies. There is also some line broadening connected with the recoil effect, but it is completely negligible

in comparison with the Doppler broadening. From Eq. (C.4) is it clear that the high-frequency lines will be most affected. Note that, in contrast to the recoil term, Doppler broadening is independent of the initial photon frequency.

To account for the effect of Doppler broadening on the final spectrum one only has to integrate Eq. (C.1) for fixed x_γ over all possible $x_{\gamma,0}$ for a given transition. The emission redshift $z_{\rm em}$ of the contribution can be found with $\nu_0/\nu = 1 + z_{\rm em}$. Afterwards, the sum over all transitions has also to be carried out, yielding the final results. To estimate the influence of the recoil effect one can simply add the recoil shift of each line to the frequency before summing over all possible transitions.

References

Bauman, R. P., Porter, R. L., Ferland, G. J., & MacAdam, K. B. 2005, ApJ, 628, 541
Beigman, I. L., & Sunyaev, R. A. 1978, preprint Leb. Phys. Inst. N163
Beigman, I. L., & Vainshtein, L. A. 2007, private communication
Benjamin, R. A., Skillman, E. D., & Smits, D. P. 1999, ApJ, 514, 307
Bennett, C. L., Halpern, M., Hinshaw, G., et al. 2003, ApJS, 148, 1
Bernshtein, I. N., Bernshtein, D. N., & Dubrovich, V. K. 1977, SvA, 21, 409
Burgin, M. S. 2003, Astron. Rep., 47, 709
Cann, N. M., & Thakkar, A. J. 2002, J. Phys. B At. Mol. Phys., 35, 421
Chluba, J., & Sunyaev, R. A. 2006a, A&A, 458, L29
Chluba, J., & Sunyaev, R. A. 2006b, A&A, 446, 39
Chluba, J., & Sunyaev, R. A. 2007a, ArXiv Astrophysics e-prints
Chluba, J., & Sunyaev, R. A. 2007b, ArXiv e-prints, 707
Chluba, J., & Sunyaev, R. A. 2007c, ArXiv e-prints, 705
Chluba, J., Rubiño-Martín, J. A., & Sunyaev, R. A. 2007, MNRAS, 374, 1310
Cunto, W., Mendoza, C., Ochsenbein, F., & Zeippen, C. J. 1993, A&A, 275, L5
Cyburt, R. H. 2004, Phys. Rev. D, 70, 023505
Drake, G. W. F. 1986, Phys. Rev. A, 34, 2871
Drake, G. W. F. 1996, Atomic, Molecular and Optical Physics Handbook, ed. G. W. F. Drake (Woodbury: AIP)
Drake, G. W. F., & Morton, D. C. 2007, ApJS, 170, 251
Drake, G. W. F., Victor, G. A., & Dalgarno, A. 1969, Phys. Rev., 180, 25
Dubrovich, V. K. 1975, SvA Lett., 1, 196
Dubrovich, V. K., & Shakhvorostova, N. N. 2004, Astron. Lett., 30, 509
Dubrovich, V. K., & Stolyarov, V. A. 1995, A&A, 302, 635
Dubrovich, V. K., & Stolyarov, V. A. 1997, Astron. Lett., 23, 565
Grachev, S. I. 1989, Astrophysics, 30, 211
Hahn, T. 2004, ArXiv High Energy Physics e-prints
Hirata, C. M., & Switzer, E. R. 2007, ArXiv Astrophysics e-prints
Hu, W., Scott, D., Sugiyama, N., & White, M. 1995, Phys. Rev. D, 52, 5498
Karzas, W. J., & Latter, R. 1961, ApJS, 6, 167
Kholupenko, E. E., & Ivanchik, A. V. 2006, Astron. Lett., 32, 795
Kholupenko, E. E., Ivanchik, A. V., & Varshalovich, D. A. 2005, Gravitation and Cosmology, 11, 161
Kholupenko, E. E., Ivanchik, A. V., & Varshalovich, D. A. 2007, MNRAS, 378, L39
Łach, G., & Pachucki, K. 2001, Phys. Rev. A, 64, 042510
Mihalas, D. 1978, Stellar atmospheres, 2nd Ed. (San Francisco: W. H. Freeman and Co.), 650
Olive, K. A., & Steigman, G. 1995, ApJS, 97, 49
Peebles, P. J. E. 1968, ApJ, 153, 1
Pozdniakov, L. A., Sobol, I. M., & Sunyaev, R. A. 1979, A&A, 75, 214
Rubiño-Martín, J. A., Chluba, J., & Sunyaev, R. A. 2006, MNRAS, 371, 1939
Rybicki, G. B., & dell'Antonio, I. P. 1993, in Observational Cosmology, ed. G. L. Chincarini, A. Iovino, T. Maccacaro, & D. Maccagni, ASP Conf. Ser., 51, 548
Rybicki, G. B., & dell'Antonio, I. P. 1994, ApJ, 427, 603
Seager, S., Sasselov, D. D., & Scott, D. 2000, ApJS, 128, 407
Smits, D. P. 1996, MNRAS, 278, 683
Storey, P. J., & Hummer, D. G. 1991, Computer Physics Communications, 66, 129
Sunyaev, R. A., & Chluba, J. 2007, ArXiv e-prints, 710
Sunyaev, R. A., & Titarchuk, L. G. 1980, A&A, 86, 121
Sunyaev, R. A., & Zeldovich, Y. B. 1970, Ap&SS, 7, 3
Switzer, E. R., & Hirata, C. M. 2007a, ArXiv Astrophysics e-prints
Switzer, E. R., & Hirata, C. M. 2007b, ArXiv Astrophysics e-prints
Wong, W. Y., & Scott, D. 2007, MNRAS, 375, 1441
Wong, W. Y., Seager, S., & Scott, D. 2006, MNRAS, 367, 1666
Zeldovich, Y. B., & Sunyaev, R. A. 1969, Ap&SS, 4, 301
Zeldovich, Y. B., Kurt, V. G., & Syunyaev, R. A. 1968, Z. Eksperimental noi i Teoreticheskoi Fiziki, 55, 278